FDTD ANALYSIS OF
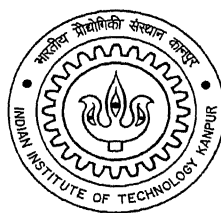
NRD GUIDE DISCONTINUITIES

By

G.V.R. Anand

DEPARTMENT OF ELECTRICAL ENGINEERING

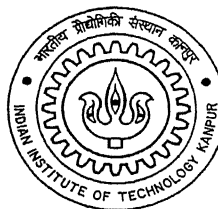# INDIAN INSTITUTE OF TECHNOLOGY, KANPUR

NOVEMBER, 2000

FDTD Analysis of

NRD Guide Discontinuities

A Thesis Submitted

in Partial Fulfillment of the Requirement
for the Degree of

MASTER OF TECHNOLOGY

by

G.V.R. Anand

to the

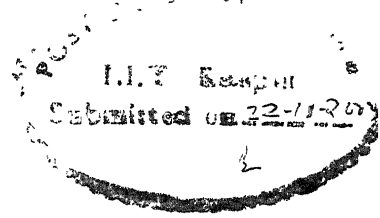## DEPARTMENT OF ELECTRICAL ENGINEERING

INDIAN INSTITUTE OF TECHNOLOGY KANPUR

November, 2000

133617

CERTIFICATE

It is certified that the work contained in the thesis entitled **FDTD Analysis of NRD guide discontinuities** by **G.V.R. Anand (Roll number 9820403),** has been carried out under my supervision and this work has not been submitted elsewhere for a degree.

Dr. M. Sachidananda

Professor

Department of Electrical Engineering,

Indian Institute of Technology, Kanpur.

22 November, 2000

Abstract

The rigorous theoretical approach for the analysis of waveguide discontinuities is difficult, as the modes excited in the vicinity of the discontinuity cannot be predicted. Alternative is to use a computational technique to approximate the behavior of the discontinuity. The Finite Difference Time Domain (FDTD) technique is used to analyse a few Non Radiative Dielectric (NRD) waveguide discontinuities. The three-dimensional FDTD formulation in cartesian coordinate system is done for the analysis of three NRD discontinuities, open-end, end-coupled gap and the edge-coupled gap discontinuity for millimeter wave frequencies centered at 35 GHz. NRD guides with Alumina ($\varepsilon_r = 9.5$) are considered in the analysis. NRD guide dimensions for Alumina, Fused quartz ($\varepsilon_r = 3.8$) and Teflon ($\varepsilon_r = 2.1$) are calculated for 15 - 85 GHz. and tabulated. An FDTD code is written based on the Yee algorithm. Maxwell's equations are discretized using the central differencing scheme for the differential equations. Code written for the simulation is first tested for the problem of diffraction of an incident TM wave by a square shaped conducting obstacle. The results obtained are compared with the published results for a similar problem. The end-coupled gap NRD guide discontinuity is analysed next. The simulation is performed for two different gap widths From the time-domain data stored through simulation, frequency dependent scattering parameters of the discontinuity are obtained over the frequency range of 33 – 37 GHz. The analysis of the edge-coupled gap discontinuity is carried for two different coupling lengths. Several modifications that could be done to the code are listed.

.

to my parents

ACKNOWLEDGEMENTS

Contents

List of Figures

List of Tables

Glossary of Symbols

Abbreviations

ABC	Absorbing Boundary Condition.
CAD	Computer Aided Design.
FDTD	Finite Difference Time Domain.
FEM	Finite Element Method.
LSE	Longitudinal-Section Electric.
LSM	Longitudinal-Section Magnetic.
NRD	Non Radiative Dielectric.

Symbols

a	Width of an NRD guide.
b	Thickness of the dielectric strip.
l	Length of the NRD guide.
m	Length of the dielectric strip inside the guide.
w	Width of the front-face (along the thickness).
p	gap length.
q	Coupling length.
Δ	Space step.

Δt	Time step.
$V_{\max}$	Maximum velocity of wave.
f	Frequency.
S	Stability factor.
γ	Propagation constant.
α	Attenuation constant.
β	Phase constant.
φ_h	Scalar function.
$\overline{E}, \ \overline{H}$	Electric and magnetic field vectors.
Π_e	Electric Hertzian potential.
Π_h	Magnetic Hertzian potential.
ω	Angular frequency.
ε	Electric permittivity.
μ	Magnetic permeability.
TE	Transverse Electric.
TM	Transverse Magnetic.
ε_r	Relative dielectric constant

Chapter 1

Introduction

1.1 Introduction

Numerical solutions of Maxwell's equations for the modeling of guided-wave passive components have been an important topic in the field of electromagnetics over the past two decades. The necessity of such activities has become increasingly obvious in recent years due to increased research and development in millimeter-wave integrated circuits and monolithic integrated circuits. Very accurate characterization methods are needed to model the structures at millimeter wave frequencies because of short wavelength.

Circuit designers would like to use CAD packages, which in most cases consist of curve fitting or empirical formulas. However, the validity of these formulas must be supported by accurate characterizations. In addition, any numerical method for characterizations need to be as efficient and economical as possible in both CPU time and temporary storage requirements, although recent rapid advances in computers impose less severe restrictions on the efficiency and the economy of the method. Another important aspect in the development of numerical methods is the trade-off among accuracy, speed, storage requirement, versatility, etc., and is often structure dependent. With the advent of microwave

integrated circuits, a number of methods have been invented and somewhat more classical methods have been refined for these modern structures.

Realizing the limitations of frequency-domain integral equation solutions of Maxwell's equations, several research organizations made explorations of an alternative approach, namely the direct time-domain solutions of Maxwell's differential equations on spatial grids or lattices. The Finite Difference Time Domain (FDTD) methods, introduced by Yee in 1966 [1], was the first technique in this class, and has gained extreme popularity over the years. In FDTD technique, the problem physical space is divided into a number of cuboids of size $\Delta x \times \Delta y \times \Delta z$ called Yee's cells. The time is discretized with interval size Δt. The excitation is performed next. The wave launched thereby is studied for its propagation behavior. The stabilized time response is numerically processed to determine the time-domain and the frequency-domain characteristics of the structures This procedure is described in detail in chapter 3.

As the modeling capabilities afforded by FDTD have become more and more popular, the interest in this area has expanded widely, making forays into technologies like cellular phones, computers, lasers and photonic circuits.

As Taflove and Hagness [2] say in their book there are seven primary reasons for the expansion of interest in FDTD and related computational solution approaches for Maxwell's equations. They are listed below. (Reproduced from [2] pp. 3-5.).

1. ***FDTD uses no linear algebra***. Being a fully explicit computation, FDTD avoids the difficulties with linear algebra that limit the size of the frequency –domain integral-equation and finite-element electromagnetics models to generally fewer than 10^6 electromagnetic field unknowns. FDTD models with as many as 10^9 field unknowns have been run; there is no intrinsic upper bound to this number.

2. ***FDTD is accurate and robust***. The sources of error in FDTD calculations are Well understood, and can be bounded to permit accurate models for a very large variety of electromagnetic wave interaction problems.

3. ***FDTD treats impulsive behavior naturally***. Being a time-domain technique, FDTD directly calculates the impulsive response of an electromagnetic system. Therefore, a single FDTD simulation can provide either ultra wide-band temporal waveforms or the sinusoidal steady-state response at any frequency within the excitation spectrum

4. ***FDTD treats nonlinear behavior naturally***. Being a time-domain technique, FDTD directly calculates the nonlinear response of an electromagnetic system.

5 ***FDTD is a systematic approach***. With FDTD, specifying a new structure to be modeled is reduced to a problem of mesh generation rather than the potentially complex reformulation of an integral equation. For example, FDTD requires no calculation of structure dependent Green's functions.

6. ***Computer memory capacities are increasing rapidly***. While this trend positively influences all numerical techniques, it is of particular advantage to FDTD methods, which are founded on discretizing space over a volume, and therefore inherently require a large random access memory.

7. ***Computer visualization capabilities are increasing rapidly***. This is of particular advantage to FDTD methods, which generate time-marched arrays of field quantities suitable for use in color videos to illustrate the field dynamics.

1.2 The Non Radiative Dielectric (NRD) waveguide

It is well known that in ordinary rectangular waveguides, the separation between the parallel plates should be an integral multiple of half the guide wavelength so that propagation of electromagnetic waves with electric field parallel to the plates to be possible. However, the cut-off is lowered if dielectric strips of proper dielectric constants are brought in. This is shown in figure 2.1. Outside the strip the waves decay exponentially. This structure is known as the Non Radiative Dielectric (NRD) waveguide. The modes that propagate in NRD guides are hybrid in nature and are called Longitudinal-Sectional Electric (LSE) and Longitudinal-Sectional Magnetic (LSM) modes. In LSE modes, the electric field is parallel to the dielectric-air boundary whereas in LSM modes the magnetic

field is parallel to the dielectric-air interface. Both LSE and LSM modes are in fact TE to x and TM to x mode fields, where x is the direction normal to the dielectric-air interface. The properties and the design of NRD guides are given in the second chapter.

1.3 Discontinuities

Practical waveguides or transmission media consist of 'discontinuities' such as diaphragms, metallic posts, dielectric slabs etc. Their purpose is to achieve the matching of a waveguide to a load or a termination, obtain a required phase shift, or for other reasons [18]. The presence of a discontinuity implies the excitation of higher order modes in its vicinity, which give rise to a phase shift in the reflected and transmitted waves and an impedance transformation at the discontinuity. Hence it is very difficult to obtain the rigorous solution of Maxwell's equations for the field distribution near the discontinuity. To describe the effect of discontinuity on the propagating mode, we need to know the modulus and phase of the reflection and transmission coefficients. Another approach is to describe the discontinuity by an equivalent transmission line circuit, which would give rise to a reflected and transmitted wave of magnitude proportional to reflection and transmission coefficient respectively. One useful method to achieve this is the variational approach, which is described in [18] for inhomogeneously filled rectangular waveguides. Computational methods such as the FDTD technique, method of lines, and Finite Element Method (FEM) etc., are popularly applied to waveguide, stripline, and microstrip discontinuities. The FDTD technique is the most popular among these. In the present work we adopted the FDTD technique for the analysis of Non Radiative Dielectric (NRD) discontinuities.

1.4 Choice of FDTD to NRD guides

When a specific structure is analyzed, one has to make a choice as to which method is best suited for the structure. Obviously, the choice is not unique. In the thesis, we investigated the behavior of some simple NRD discontinuities with the

finite difference time-domain method. The choice of FDTD to NRD was based on the following reasons:

- Two infinitely conducting plates at the top and bottom confine the NRD guides. This simplifies the boundary conditions in one of the directions.

- One of the complexities in FDTD approach was its applicability to curved boundaries. The discontinuities we considered in the thesis are straight.

- Many EM structures have open boundaries extending up to infinity. As we cannot have infinite computing domain, we need to truncate it by applying Absorbing Boundary Conditions (ABCs) (To be discussed in Chapter 2.) on those boundaries. Some problems require very complex ABCs in two or three dimensions, which make the FDTD formulation tedious. In the NRD guides, however, the fields decay rapidly outside the strip going down by as much as 20 dB from the maximum, at relatively smaller distances outside the dielectric strip. This paves the way for a less stringent requirement of ABCs on the NRD guides as explained later.

1.5 Literature Survey

The number of research publications on NRD guides is very few. The paper by Yoneyama and Nishida [16] is the first on NRD guides. They introduced the non radiative dielectric (NRD) waveguide in the paper and explained the principle operation. The condition of single mode operation is explained along with the design diagrams. Although they have given the design data for various NRD components such as T-junctions, Right-angle corner, Directional coupler, they did not give the measured results in the paper.

Yoneyama, Tozawa and Nishida [17] have presented an approximate analytical method for predicting coupling characteristics of dielectric strips in the non radiative dielectric waveguide. They found that the coupling coefficient of NRD guide is large compared to those of other dielectric waveguides. They used polysterene bends having a curvature radius of 20 mm at 50 GHz. The theory presented is also verified experimentally. Dawn and Sachidananda [19] have

done a rigorous analysis to derive the field expressions for the various modes of propagation in NRD guides. Also presented is the excitation of NRD waveguides.

The Finite Difference Time Domain (FDTD) method was first introduced by Yee [1] in 1966. He discretized the Maxwell's equations by a set of finite difference equations. Yee also gave expressions for the stability criterion, which deals with the space and time discretization values to be chosen for the FDTD simulation to be stable. There was an error in the 3-D stability expressions he gave which were later corrected by Taflove and Brodwin [4]. An example of the scattering of an electromagnetic wave by a perfectly conducting obstacle is given. The theoretical and FDTD simulation results are in good agreement. The book by Taflove and Hagness [2] has an exhaustive coverage of topics on the FDTD technique. Peterson, Ray and Mittra [20] cover various methods in computational electromagnetics. The book has a chapter on the FDTD technique. A selective survey of FDTD literature can be found in [3]. Taflove and Brodwin [4] investigated the solution of electromagnetic fields within an arbitrary dielectric scatterer of the order of one wavelength in diameter. They have also outlined the procedure for the extension of this method to three-dimensional dielectric scatterers. Zhang and Mei [5] have described the procedure of obtaining the frequency-dependent characteristics of microstrip discontinuities from the time-domain results obtained through FDTD simulation. The choice of the excitation for a given electromagnetic structure is also explained. Special boundary conditions such as the dielectric-air boundary conditions are explained and relevant conditions are provided.

If the problem under analysis has open boundaries, then special consideration is needed on those boundaries, as one cannot have infinite computing domain. The need then arises for absorbing boundary conditions (ABCs). ABCs are of two types: analytical and material absorbing boundary conditions. Enquist and Mazda [6] first proposed the analytical ABCs. Later, Mur [7] optimized them and presented them in modified form. In analytical ABCs the reflection of the outgoing numerical waves is kept within an acceptable limit by imposing certain conditions on the field components at the boundaries. An

alternate approach to realize an ABC is to terminate the outer boundary of the space lattice in an absorbing material medium [2]. This is analogous to the physical treatment of the walls of an anechoic chamber. Ideally, the absorbing medium is only a few lattice cells thick, reflectionless to all impinging waves over their full frequency spectrum, highly absorbing and effective in the near field of a source scatterer. We have used the Mur's ABC in the present work.

The FDTD technique has been applied to a variety of microstrip circuits over the last two decades. Zhang, Fang, Mei and Liu [9] have made calculations of the dispersive characteristics of microstrips by the FDTD method. Sheen, Ali, Abouzahra and Kong [10] presented a procedure for the analysis of microstrip circuits through the 3-D FDTD technique. They applied the technique to rectangular microstrip antenna, microstrip low-pass filter and a branch-line coupler. In all the three cases they have given the scattering parameters as a function of frequency.

The application of the FDTD method becomes tedious when the structure under analysis has curved boundaries. With rectangular Yee cells, one can make a staircase approximation to the curved boundary. But this is not always precise. In such an eventuality one can opt for the FDTD formulation in spherical or cylindrical coordinate system. The paper by Chen, Mittra and Harms [11] presents the FDTD algorithm for solving the Maxwell's equations in rotationally symmetric geometries. The analysis becomes more complex when the given structure has both straight as well as curved boundaries as no single coordinate system can yield accurate results. An alternative is to go for a sub-gridding technique proposed by Zivanovic, Yee and Mei [12]. In this technique, a fine grid is chosen in curved regions and a coarse grid is chosen for other regions in the structure. Note that in sub-gridding technique, different regions have different grid spacing and there is an abrupt transition in the step at the boundaries of the reasons. A non-uniform FDTD algorithm was proposed by Shen, Chen and Mittra [13]. Here, the grid spacing can be varied gradually with distance in the structure. They applied this technique to optical-fiber waveguides.

The FDTD technique is an approximation method. Some problems may require high accuracy in field calculations. Hadı, picket-May [14] discussed a higher order accuracy model of FDTD technique. They have used finite difference equations of higher accuracy to achieve this. The reduction in dispersion by the use of the higher order scheme is described in [15].

A comprehensive database of FDTD literature including the latest list of publications, books, journals and surveys can be found on the internet at the site: http://www.fdtd.org

1.6 Organization of the thesis

The thesis has been organized into five chapters. In chapter 2, an introduction to waveguide discontinuities and the Non Radiative Dielectric (NRD) waveguides is given. The properties and mode structure of the NRD guides are given. The design data for the NRD guides in the frequency range 10 – 85 GHz. has been calculated and tabulated for Alumina , Fused quartz and Teflon dielectric strips. The various discontinuities analyzed in the thesis are described and the design parameters are given.

The third chapter has a detailed treatment of the FDTD technique. In the FDTD formulation part, the expressions used for the discretization of differential equations are given. Central differencing scheme has been used in our investigation. Using these expressions, the discretization of the Maxwell's equations has been carried out and the resulting individual expressions for all the electric and magnetic field components in the Cartesian co-ordinate system are listed. The conditions on the space and time step values to be taken in the FDTD simulation are stated next and are followed by the source considerations. Open boundaries on a structure need special treatment, as one cannot have infinite computing domain. The Absorbing Boundary Conditions (ABCs), which are nothing but the analytical simulation of the electric fields on the boundary as plane waves with zero reflection coefficients, serve the purpose. Derivations are given for the analytical ABCs introduced by Mur [7], which, we have used in the

present work. Other ABCs, which use material boundaries, are discused. Extraction of the frequency-domain results from the time-domain data through the Fourier transforming techniques is described next. Also given is the procedure for obtaining the S-parameters.

The fourth chapter deals with the simulation and the results. First, the code has been tested for a simple 2-dimensional test case taken from [1] and the results from our code as well as those from [1] are given. Next the FDTD simulation has been carried out for the open, end-coupled and the edge-coupled NRD guide discontinuities and the frequency dependent scattering parameters are given for each discontinuity are given. The summary and scope for future work have been presented in the fifth chapter.

`

Chapter 2

Analysis of NRD discontinuities

2.1 Introduction

Practical waveguides or transmission media consisting of 'discontinuities' such as diaphragms, metallic posts, dielectric slabs etc. whose purpose is to achieve the matching of a waveguide to a load or a termination, obtain a required phase shift, or for other reasons [18]. The presence of a discontinuity implies the excitation of higher order modes in its vicinity, which give rise to a phase shift in the reflected and transmitted waves and an impedance transformation at the discontinuity. Hence it is very difficult to obtain the rigorous solution of Maxwell's equations for the field distribution near the discontinuity. To describe the effect of discontinuity on the propagating mode, we need to know the modulus and phase of the reflection and transmission coefficients. Another approach is to describe the discontinuity by an equivalent transmission line circuit, which would give rise to a reflected and transmitted wave of magnitude proportional to reflection and

transmission coefficient respectively. One useful method to achieve this is the variational approach, which is described in [18] for inhomogeneously filled rectangular waveguides. Computational methods such as the FDTD technique and FEM are popularly applied to waveguide, stripline and microstrip discontinuities. In the present work we adopted the FDTD technique for the analysis of Non Radiative Dielectric (NRD) discontinuities.

2.2 The Non Radiative Dielectric (NRD) waveguide

In this section, we discuss the Non Radiative Dielectric (NRD) waveguide [16,17], which consists of a dielectric strip of rectangular cross section, sandwiched between two parallel conducting plates. Most of the electromagnetic energy is concentrated in the dielectric strip. Only a small fraction of electromagnetic energy is transported outside the dielectric but between the plates.

In ordinary waveguides, the separation between the parallel plates should be an integral multiple of half wavelength for the propagation of electromagnetic waves with electric field parallel to the plates possible. However, if dielectric strips of proper dielectric constants are brought in, as shown in figure 2.1, the cut-off is eliminated and the propagation along the strip takes place, irrespective of whether they are straight or curved. Outside the strip the waves decay exponentially.

At the lower end of the millimeter wave spectrum, the use of microstrips, slot lines, and fin lines are common, but conduction losses among these printed transmission lines tend to increase drastically with higher operating frequencies. So, less lossy guiding media are being studied with the expectation of realizing high performance millimeter wave integrated circuits. Dielectric waveguide configurations have been investigated for fulfilling such a low loss requirement,

as excellent dielectric materials with loss tangents as small as 10^{-4} are available in the millimeter wave frequency range.

The NRD guide is a dielectric waveguide structure, which can completely suppress radiation at curved sections and discontinuities, without spoiling the low loss nature of dielectric waveguide. In contrast to commonly used rectangular/circular waveguides, a small part of the energy is transported outside the guide. Most of the energy travels along the dielectric strip.

The NRD guide has some valuable properties:

1. The attenuation, which is lower than that of a conventional rectangular waveguide, decreases continuously with increasing frequency for the dominant mode.

2. Since NRD fields decay very fast outside the dielectric strip, bends and discontinuities can be easily incorporated in complicated integrated circuits, with very little radiation. This is one of the principal advantages of NRD guides.

3. Simple production processes using NRD guides can fabricate complicated microwave or millimeter wave circuitry. The simplicity of fabrication is one of the most important advantages for NRD guide. The derived field expressions for the LSM_{01} mode show that the field strength distribution has no component of the magnetic field perpendicular to the direction of wave propagation, in the vicinity of the conducting plates. So it follows that no currents occur in longitudinal direction on the conducting plates and therefore the wave propagation is unaffected by slots and gaps in the conducting plates, transverse to the direction of propagation. Therefore conductors and flanges used to join NRD guide sections are not critical.

4. The conventional rectangular waveguides are expensive and difficult to fabricate. They also have higher losses than an NRD guide. The low

losses make the NRD guide suitable for frequencies in millimeter wave region

The configuration of an NRD guide is shown in Fig. 2.1. It consists of a dielectric strip of relative permitivity ε_r sandwiched between parallel perfectly conducting plates. The propagation properties are found by applying boundary conditions at the top and bottom conducting plates as well as the dielectric-air interfaces. The fields in the guide are determined from the magnetis or electric Hertzian potential depending on the mode under investigation. The NRD-guide structure supports two types of surface-wave modes, LSE_{mn} and LSM_{mn} [18]. The designation LSE stands for Longitudinal-Section Electric field. where the electric field is parallel to the dielectric air interface and LSM stands for Longitudinal-Section Magnetic field, where the magnetic field is parallel to the dielectric-air interface. The LSE and LSM modes are hybrid in nature and they can be represented in terms of TE and TM mode fields.

2.3 Design of NRD guides

As said, the LSE and LSM modes are hybrid in nature and can be expressed in terms of TE and TM mode fields. Consider the fig. 2.1. For TE modes we have $E_z = 0$. Assuming a magnetic Hertzian potential $\vec{\Pi}_h = \hat{z}\Pi_{hz}$ we can derive the required fields from the following equations [19]

$$\vec{E} = -j\omega\mu\nabla\times\vec{\Pi}_h \quad , \tag{2.1}$$

$$\vec{H} = \nabla\times\nabla\times\vec{\Pi}_h \quad , \tag{2.2}$$

Where, $\vec{\Pi}_h$ is a solution of the Helmholtz equation

$$\nabla^2\vec{\Pi}_h + k^2\vec{\Pi}_h = 0 \quad , \tag{2.3}$$

With $\quad \vec{\Pi}_h = \hat{z}\varphi_h(x,y)\ e^{-\gamma z} \quad , \tag{2.4}$

and $\quad k^2 = \omega^2\mu\varepsilon .$

13
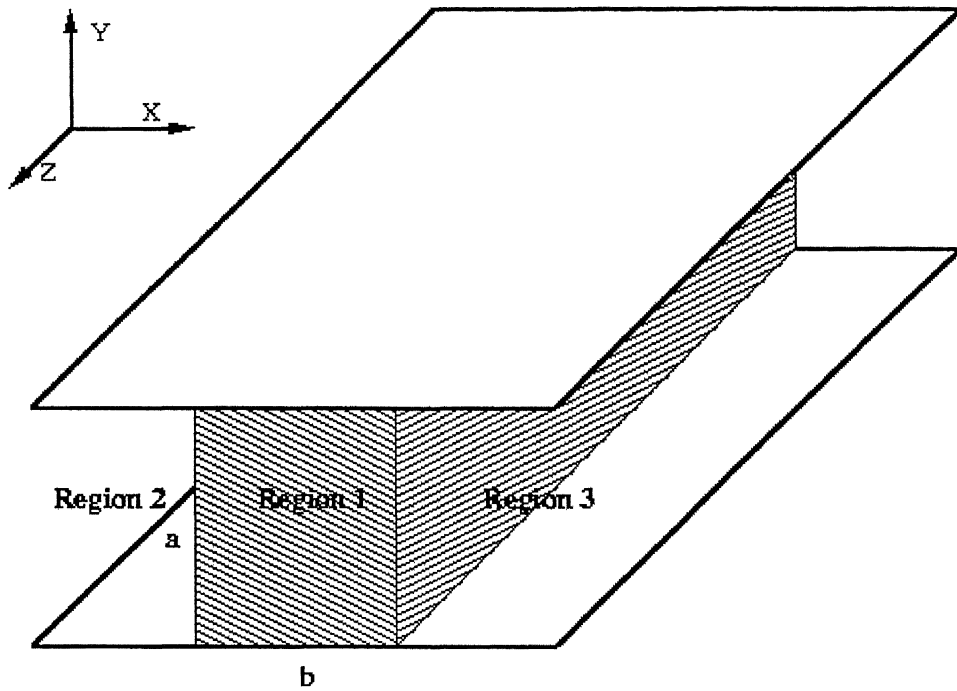
Fig. 2.1 The non radiative dielectric waveguide

where $\gamma = \alpha + j\beta$, the propagation constant with α and β being the attenuation and phase constants respectively. ψ_h is a scalar function. Referring to fig. 2.1 we have three different regions of analysis: Region 1 with a relative permittivity of ε_r and regions 2 and 3 which are air-filled. Conducting plates of infinite length bound all the three regions. The TE mode fields are obtained by solving the scalar Helmholtz equation, which gives ψ_h.

Similar is the case with TM modes. Here $H_z = 0$, and the fields are derived from electric Hertzian potential $\Pi_e = \hat{z}\psi_e(x,y)e^{-\gamma z}$ through the equations:

$$\vec{E} = \nabla \times \nabla \times \vec{\Pi}_e \qquad\qquad (2.5)$$

$$\vec{H} = j\omega\varepsilon\nabla \times \vec{\Pi}_e \qquad\qquad (2\ 6)$$

Where $\quad \vec{\Pi}_e = \hat{z}\psi_e(x,y)e^{-\gamma z} \qquad\qquad (2.7)$

and $\quad \nabla^2\vec{\Pi}_e + k^2\vec{\Pi}_e = 0 \qquad\qquad (2.8)$

We see that ψ_e also satisfies the scalar Helmholtz equation (2.8). Solving this equation gives the TM mode fields.

In order to satisfy the dielectric-air boundary conditions in NRD guides we need to have a combination of TE and TM modes as the individual fields do not satisfy them. As discussed, these hybrid modes are called LSE, LSM modes and are a combination of TE and TM modes. For obtaining the propagation constant of these hybrid LSE and LSM modes, the required characteristic equations are found by applying the condition that for LSM modes $H_x = 0$ and for LSE modes $E_x = 0$ on the dielectric air boundary in fig. 2.1. The field structure of LSE$_{01}$ and LSM$_{01}$ is shown in figures 2.2 and 2.3 respectively

The rigorous theoretical analysis for the NRD guides can be found in [19] and [16]. A limited NRD design data (dimensions) for NRD guides containing alumina ($\varepsilon_r = 9.5$) as the dielectric can be found in [16]. The design data for a finer range frequencies for alumina fused quartz ($\varepsilon_r = 3.8$) and Teflon ($\varepsilon_r = 2.1$) is given tables 2.1, 2.2 and 2.3 respectively.
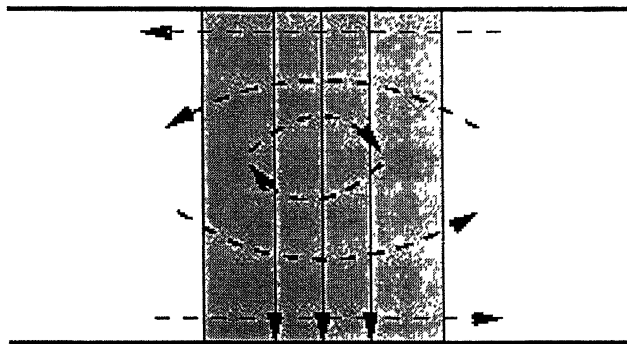
Fig. 2.2 LSE_{01} mode in NRD guides.
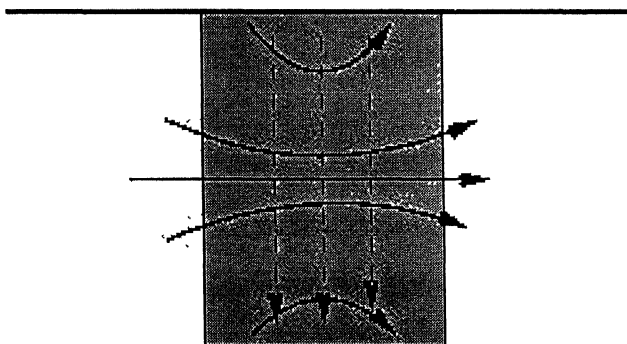
Fig. 2.3 LSM_{01} mode in NRD guides.

Table 2.1 NRD guide dimensions for Alumina (ε_r=9.5)

Description	Frequency (GHz.)	Width **a** mm	Thickness **b** mm
NRD guide (Alumina) $\varepsilon_r = 9.5$ $\dfrac{a}{\lambda_0} = 0.45$ $\dfrac{\sqrt{\varepsilon_r - 1}}{\lambda_0} b = 0.45$	9-11	13.50	4.63
	13.5-16 5	8.99	3.08
	18-22	6.74	2.31
	22-27	5.39	1.85
	27-33	4.50	1.54
	31-38	3.86	1.32
	36-44	3.37	1.16
	41-49	3.00	1.02
	45-55	2.70	0.92
	50-60	2.45	0.84
	54.5-65.5	2.25	0.77
	59-71	2.07	0.71
	64-76	1.93	0.66
	68-82	1.80	0.62
	73-87	1.69	0.58
	77-96	1.58	0.54

Table 2.2 NRD guide dimensions for Fused quartz. (ε_r= 3.8)

Description	Frequency (GHz.)	Width **a** mm	Thickness **b** mm
NRD guide (Fused Quartz) $\varepsilon_r = 3.8$ $\dfrac{a}{\lambda_0} = 0.45$ $\dfrac{\sqrt{\varepsilon_r - 1}}{\lambda_0} b = 0.45$	9-11	13.50	8.07
	13.5-16.5	8.99	5.37
	18-22	6.74	4.02
	22-27	5.39	3.22
	27-33	4.50	2.68
	31-38	3.85	2.30
	36-44	3.37	2.02
	41-49	3.00	1.78
	45-55	2.70	1.68
	50-60	2.45	1.46
	54.5-65.5	2.25	1.34
	59-71	2.07	1.24
	64-76	1.93	1.15
	68-82	1.80	1.08
	73-87	1.69	1.01
	77-96	1.58	0.94

2.4 Discontinuities analysed

In the thesis we investigated a few NRD discontinuities by the FDTD technique. The frequency of interest was 35 GHz. The discontinuities analysed are open discontinuity, end coupled gap discontinuity and edge coupled gap discontinuity. Our primary objective in all the three cases was to obtain the frequency dependent scattering parameters for each discontinuity. NRD guides

with Alumina strips ($\varepsilon_r = 9.5$) are considered in our work. As discussed previously, outside the

Table 2.3 NRD guide dimensions for Teflon (ε_r=2.1)

Description	Center frequency (GHz.)	Width a mm	Thickness b mm
NRD guide (Teflon) $\varepsilon_r = 2.1$ $\dfrac{a}{\lambda_0} = 0.45$ $\dfrac{\sqrt{\varepsilon_r - 1}}{\lambda_0} b = 0.45$	10	13 50	12.87
	15	8 99	8 57
	20	6 74	6.41
	25	5.39	5.13
	30	4 50	4.28
	35	3.85	3.67
	40	3.37	3.22
	45	3.00	2.84
	50	2.70	2.68
	55	2.45	2.33
	60	2.25	2.14
	65	2.07	1.98
	70	1.93	1.83
	75	1.80	1.72
	80	1.69	1.61
	85	1.58	1.50

dielectric strip, the fields decay rapidly. Hence, closing the NRD guide with two more conducting plates along the thickness at a considerable distance from the center does not affect the behavior of the guide.

2.4.1 Open-end discontinuity

Figure 2 4 and 2.5 show the front view and top view with top conducting removed of a typical open-end NRD discontinuity with a dielectric strip. In the NRD guide shown, the dielectric strip extends up to some distance (*m*) along the length and the remaining part is air filled. The width of the strip is given by *a*, *b* is the thickness and *w* is the front face width. The length of the guide is given by *l*.
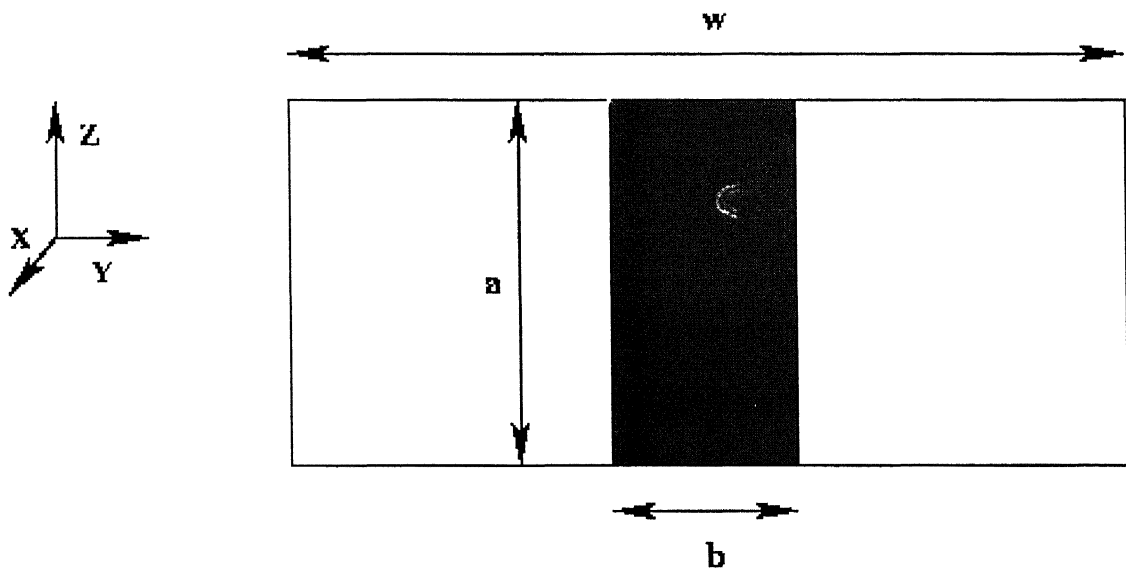
Fig. 2.4 Front-view of an open-ended NRD guide discontinuity.
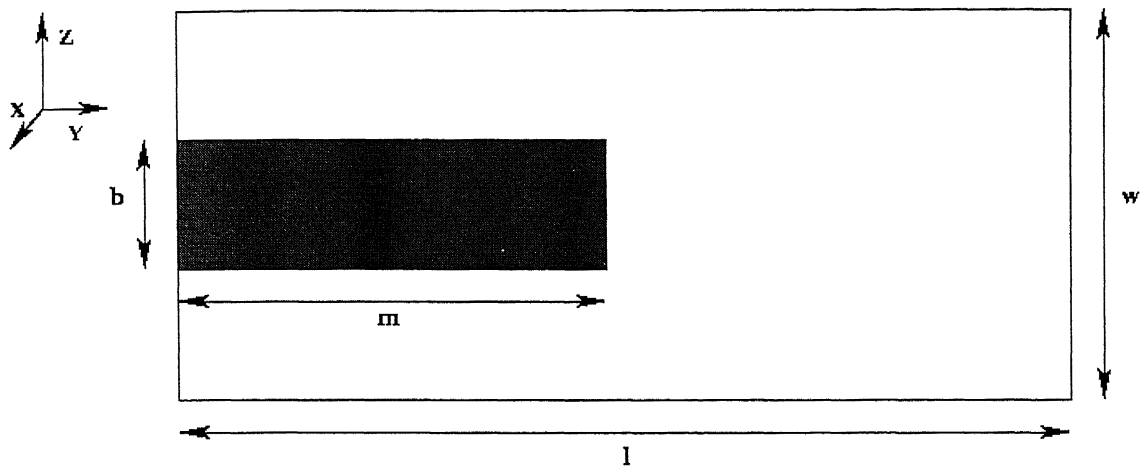
Fig. 2.5 Top view (with the top conducting plate removed) of the open-ended NRD guide discontinuity.
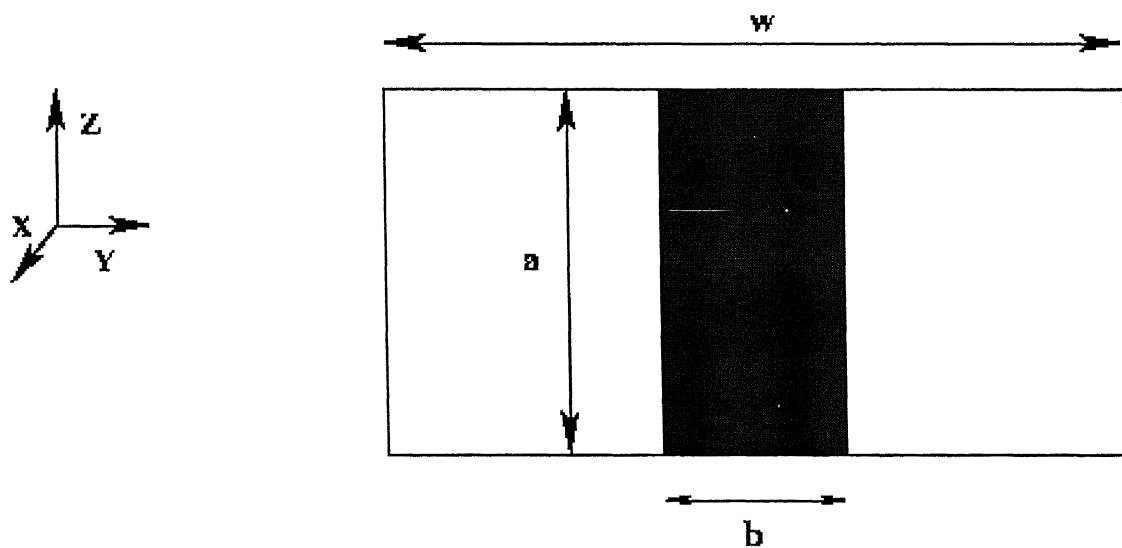
Fig. 2.6 Front-view of an end-coupled NRD gap discontinuity.

2.4.2 End-coupled gap discontinuity

The front view and the top view of an NRD guide with an end-coupled gap discontinuity with a dielectric strip are shown in figure 2.6 and figure 2.7 respectively. Varying the gap length will yield different results. The denomination of a,b,w and l is the same as follows. Additionally p stands for the gap between the strips along the length.
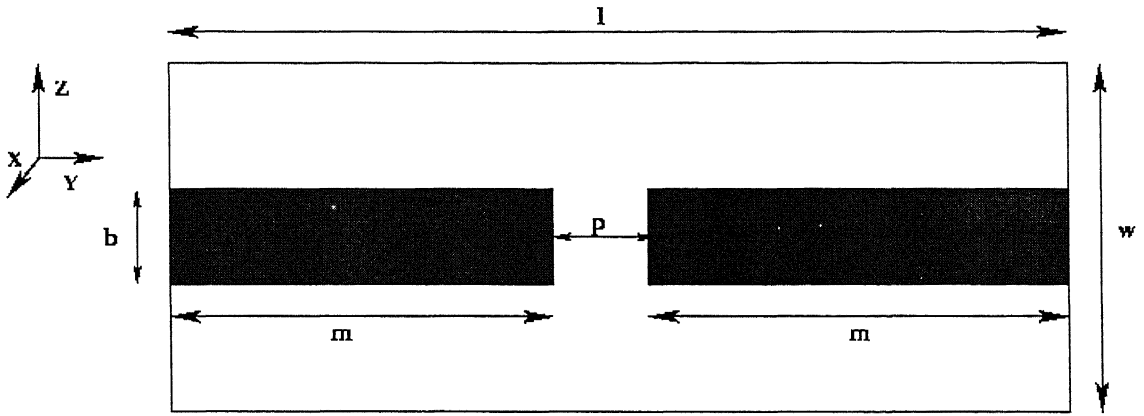
Fig. 2.7 Top view of the end-coupled NRD guide with the top conducting plate removed.

2.4.3 Edge-coupled gap discontinuity

The front view and the top view of the NRD guide with an edge-coupled gap discontinuity are shown in figures 2.8 and 2.9 respectively. All the labeling is the same as for the previous discontinuities. The additional dimension namely q stands for the edge coupling length.

22
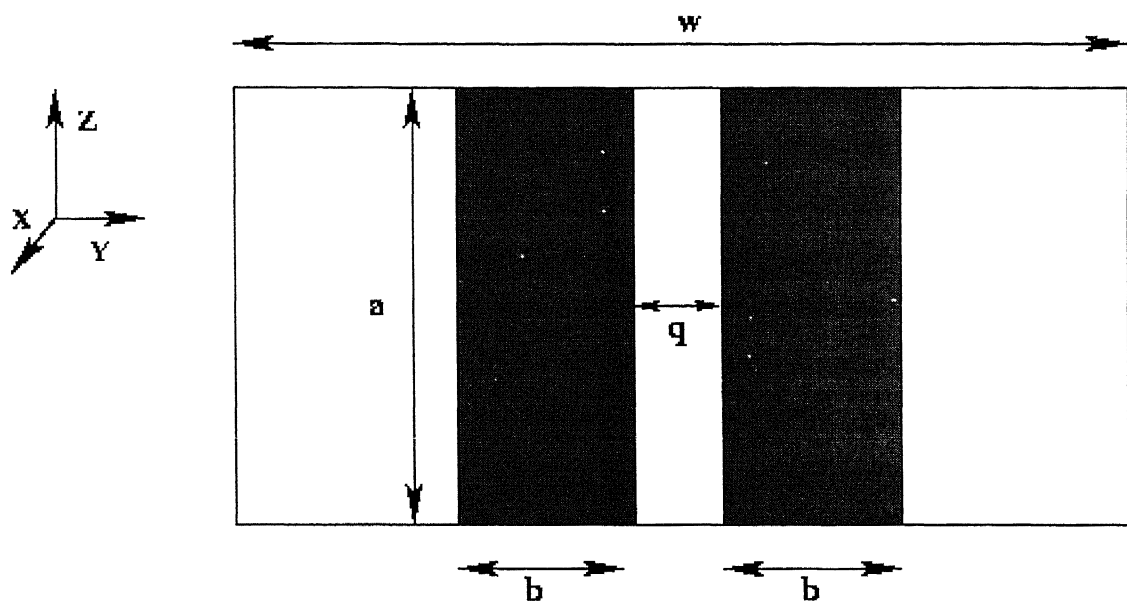
Fig. 2.8 Front view of an edge-coupled NRD guide discontinuity
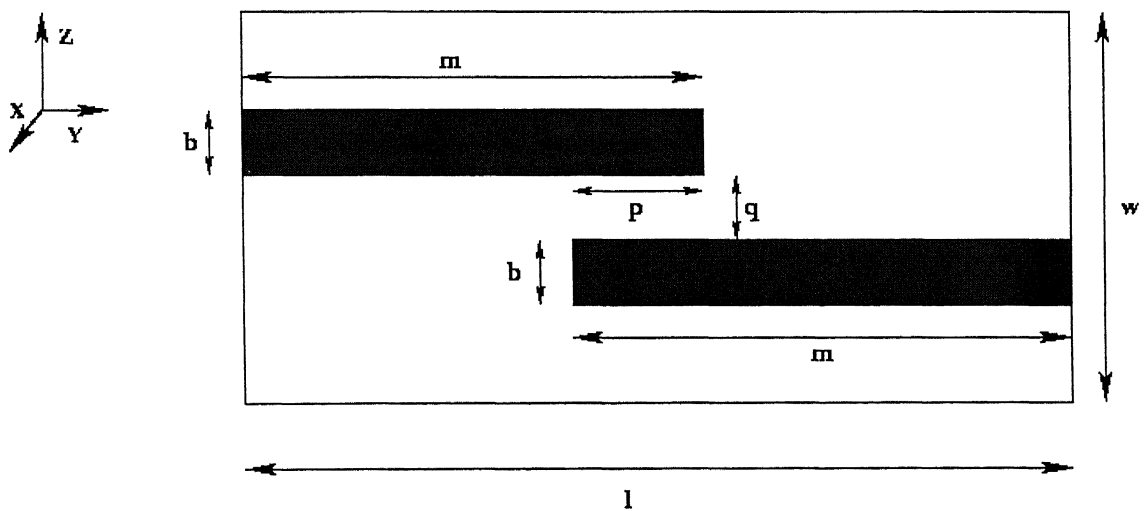
Fig. 2.9 Top view of an edge-coupled NRD guides discontinuity.

Chapter 3

The Finite Difference Time Domain (FDTD) method.

3.1 Introduction

A number of numerical techniques are available for solving electromagnetic problems. These include the integral equation technique, method of lines, mode matching, boundary integral method, differential equation approaches including finite difference time domain (FDTD) and finite element techniques. Among these techniques FDTD method is being used extensively in the following areas. It has been used for studying scattering [2-4], propagation in transmission lines, discontinuities, radiation, analysis in time domain, non-linear circuits [2] etc. The major difference between FDTD and other numerical techniques is that the analytical pre-processing and modeling is almost absent in FDTD.

As discussed in chapter 1, FDTD was proposed by Yee in 1966 [1] and has been used by many investigators because of the following advantages over other techniques:

a) From the mathematical point of view it is a direct implementation of Maxwell's curl equations. Therefore analytical processing of Maxwell's equations is almost negligible

b) It is capable of predicting broadband frequency response because the analysis is carried out in the time domain.

c) It is capable of analyzing the complex systems, including wave interaction with aircraft, human body, or satellite, non-linear device simulations, complex antennas etc.

d) It is capable of analyzing structures using different type of materials e.g., lossy dielectrics, magnetized ferrites, anisotropic plasmas, etc.

To this list the advantage of computational efficiency for large problems in comparison with other techniques such as the method of moments or finite element method can be added, especially when predicting broadband response.

One needs a digital computer ranging from PC-486 to supercomputer, depending the electrical size of the problem structure and the needed discretization size for a given accuracy. Computer resource requirement for FDTD is large for the problems, which can be analyzed using techniques involving analytical pre-processing of the problem such as integral equation, mode matching, method of lines etc.

Analysis of any problem using FDTD starts with dividing the structure into various regions based on the material properties. Unbounded region, if any, is then bounded by terminating it with absorbing medium or termination such that reflections do not occur. Next, the problem physical space is discretized in the form of a number of cuboids of size Δx, Δy, Δz. The time is also discretized with interval size Δt. The structure is then excited by an electromagnetic pulse. The wave launched by the pulse in the structure is then studied for its propagation

behavior. The stabilized time waveform is numerically processed to determine the time domain and frequency domain characteristics of the structures.

3.2 FDTD formulation

To simulate the time varying electromagnetic fields in any linear isotropic media with constant ε, μ, σ. Maxwell's curl equations are sufficient because the Maxwell's divergence equations are contained in them. The curl equations are

$$\sigma \overline{E} + \varepsilon \frac{\partial \overline{E}}{\partial t} = \nabla \times \overline{H} \qquad (3.1a)$$

$$\mu \frac{\partial \overline{H}}{\partial t} = -\nabla \times \overline{E} \qquad (3.1b)$$

Here ε and σ are the electric permittivity and the conductivity, and μ is the magnetic permeability of the medium.

In order to obtain unique solutions of (3.1), the following conditions may be specified.

a) The value of the fields at $t = 0$ must be specified on the whole domain of interest. They are assumed to be zero except at the plane of excitation.

b) The tangential components of $\overline{E}$ and $\overline{H}$ on the boundary of the domain must be given for all $t>0$.

Now, the partial differential equations (3.1) are solved subject to the conditions stated above by expressing the derivatives in terms of finite difference approximations. The central difference approximation is used for higher accuracy. It is defined as,

$$\left. \frac{\partial F}{\partial u} \right|_{u_0} = \frac{F(u_0 + \frac{\Delta u}{2}) - F(u_0 - \frac{\Delta u}{2})}{\Delta u} + O(\Delta u)^2 . \qquad (3.2)$$

Equation (3.2) implies that the $\overline{E}$ and $\overline{H}$ fields should be known at discrete points (x_l, y_m, z_n) only, where $x_l = l\Delta x$, $y_m = m\Delta y$ and $z_n = n\Delta z$ with Δx, Δy, Δz representing the step size. To implement the finite differencing scheme in *3-D*, the problem is divided into a number of cells called Yee cells of dimensions mentioned above. One such cell is shown in fig. 3.1. The remarkable property of this cell is that the positions of different components of $\overline{E}$ and $\overline{H}$ are chosen in such a manner that equations (2.1) are satisfied automatically. In this arrangement, $\overline{E}$ and $\overline{H}$ nodes are located such that $\overline{H}$ nodes are displaced by half a space step *($\Delta x/2$, $\Delta y/2$, $\Delta z/2$)* with respect to corresponding $\overline{E}$ nodes as shown in fig. 3.1. The time instant at which $\overline{H}$ fields are calculated are also delayed by half a time step, *$\Delta t/2$.*

Applying the central differencing scheme (equation (3.2)) to equations 3.1(a) and 3.1(b), we get the discretized field components of the Yee's cell shown in fig. 3.1. The expressions for the individual field components from (3.1) are:

$$\frac{\partial E_x}{\partial t} = \frac{1}{\varepsilon}\left(\frac{\partial H_z}{\partial y} - \frac{\partial H_y}{\partial z}\right), \qquad (3.3a)$$

$$\frac{\partial E_y}{\partial t} = \frac{1}{\varepsilon}\left(\frac{\partial H_x}{\partial z} - \frac{\partial H_z}{\partial x}\right), \qquad (3.3b)$$

$$\frac{\partial E_z}{\partial t} = \frac{1}{\varepsilon}\left(\frac{\partial H_y}{\partial x} - \frac{\partial H_x}{\partial y}\right), \qquad (3.3c)$$

$$\frac{\partial H_x}{\partial t} = \frac{1}{\mu}\left(\frac{\partial E_y}{\partial z} - \frac{\partial E_z}{\partial y}\right), \qquad (3.3d)$$

$$\frac{\partial H_y}{\partial t} = \frac{1}{\mu}\left(\frac{\partial E_z}{\partial x} - \frac{\partial E_x}{\partial z}\right), \qquad (3.3e)$$
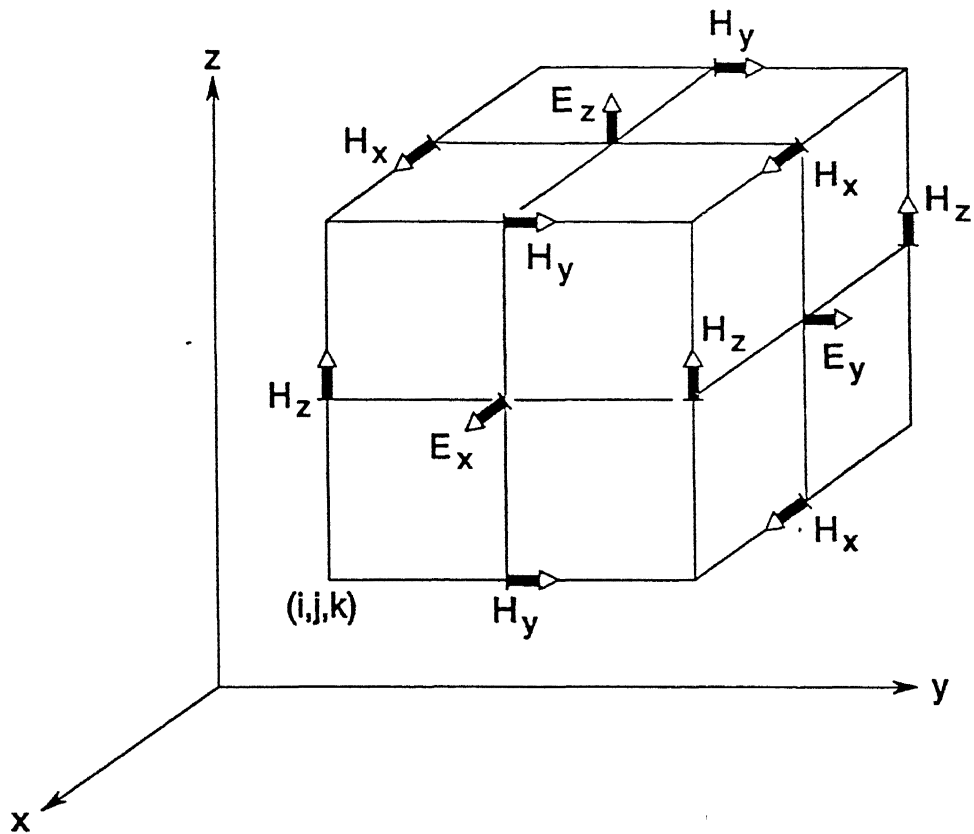
Fig. 3.1 Yee's cell [1]

$$\frac{\partial H_z}{\partial t} = \frac{1}{\mu}\left(\frac{\partial E_x}{\partial y} - \frac{\partial E_y}{\partial x}\right) \quad . \tag{3.3f}$$

Now, considering (3.3a) and discretizing it using the central differencing formula (3.2) on E_x, H_z and H_y the Yee's cell of fig 3 1, we get,

$$\frac{E_x^{n+1}(i+\frac{1}{2},j,k) - E_x^{n}(i+\frac{1}{2},j,k)}{\Delta t} = \frac{1}{\varepsilon}\left[\frac{H_z^{n+\frac{1}{2}}(i+\frac{1}{2},j+\frac{1}{2},k) - H_z^{n+\frac{1}{2}}(i+\frac{1}{2},j-\frac{1}{2},k)}{\Delta y}\right]$$

$$-\frac{1}{\varepsilon}\left[\frac{H_y^{n+\frac{1}{2}}(i+\frac{1}{2},j,k+\frac{1}{2}) - H_y^{n+\frac{1}{2}}(i+\frac{1}{2},j,k-\frac{1}{2})}{\Delta z}\right]$$

From the above expression E_x is obtained by cross multiplication and rearranging.

$$E_x^{n+1}(i+\frac{1}{2},j,k) = E_x^{n}(i+\frac{1}{2},j,k) + \frac{\Delta t}{\varepsilon\Delta y}\left(H_z^{n+\frac{1}{2}}(i+\frac{1}{2},j+\frac{1}{2},k) - H_z^{n+\frac{1}{2}}(i+\frac{1}{2},j-\frac{1}{2},k)\right)$$

$$- \frac{\Delta t}{\varepsilon\Delta z}\left(H_y^{n+\frac{1}{2}}(i+\frac{1}{2},j,k-\frac{1}{2}) - H_y^{n+\frac{1}{2}}(i+\frac{1}{2},j,k+\frac{1}{2})\right)$$

Similarly all other field components can be derived. The equations (3.4a)-(3.4f) give the complete expressions.

$$H_x^{n+\frac{1}{2}}(i,j+\frac{1}{2},k+\frac{1}{2}) = H_x^{n-\frac{1}{2}}(i,j+\frac{1}{2},k+\frac{1}{2}) + \frac{\Delta t}{\mu\Delta z}\left(E_y^{n}(i,j+\frac{1}{2},k+1) - E_y^{n}(i,j+\frac{1}{2},k)\right)$$

$$+ \frac{\Delta t}{\mu \Delta z} \left(E_z^n(i,j,k+\frac{1}{2}) - E_z^n(i,j+1,k+\frac{1}{2}) \right) , \qquad (3.4a)$$

$$H_y^{n+\frac{1}{2}}(i+\frac{1}{2},k,j+\frac{1}{2}) = H_y^{n-\frac{1}{2}}(i+\frac{1}{2},j,k+\frac{1}{2}) + \frac{\Delta t}{\mu \Delta x} \left(E_z^n(i+1,j,k+\frac{1}{2}) - E_z^n(i,j,k+\frac{1}{2}) \right)$$

$$+ \frac{\Delta t}{\mu \Delta z} \left(E_x^n(i+\frac{1}{2}),j,k) - E_x^n(i+\frac{1}{2},j,k+1) \right) , \qquad (3.4b)$$

$$H_z^{n+\frac{1}{2}}(i+\frac{1}{2},J+\frac{1}{2},k) = H_z^{n-\frac{1}{2}}(i+\frac{1}{2},j+\frac{1}{2},k) + \frac{\Delta t}{\mu \Delta y} \left(E_x^n(\imath+\frac{1}{2},j+1,k) - E_x^n(i+\frac{1}{2},j,k) \right)$$

$$+ \frac{\Delta t}{\mu \Delta x} \left(E_y^n(i,j+\frac{1}{2},k) - E_v^n(i+1,J+\frac{1}{2},k) \right) , \qquad (3.4c)$$

$$E_x^{n+1}(i+\frac{1}{2},j,k) = E_x^n(i+\frac{1}{2},j,k) + \frac{\Delta t}{\varepsilon \Delta y} \left(H_z^{n+\frac{1}{2}}(i+\frac{1}{2},j+\frac{1}{2},k) - H_z^{n+\frac{1}{2}}(i+\frac{1}{2},j-\frac{1}{2},k) \right)$$

$$+ \frac{\Delta t}{\varepsilon \Delta z} \left(H_y^{n+\frac{1}{2}}(i+\frac{1}{2},j,k-\frac{1}{2}) - H_y^{n+\frac{1}{2}}(i+\frac{1}{2},j,k+\frac{1}{2}) \right) , \quad (3.4d)$$

$$E_y^{n+1}(i,j+\frac{1}{2},k) = E_y^n(i,j+\frac{1}{2},k) + \frac{\Delta t}{\varepsilon \Delta z} \left(H_x^{n+\frac{1}{2}}(i,j+\frac{1}{2},k+\frac{1}{2}) - H_x^{n+\frac{1}{2}}(i+\frac{1}{2},j-\frac{1}{2},k) \right)$$

$$+ \frac{\Delta t}{\varepsilon \Delta x} \left(H_z^{n+\frac{1}{2}}(i-\frac{1}{2},j+\frac{1}{2},k) - H_z^{n+\frac{1}{2}}(i+\frac{1}{2},j+\frac{1}{2},k) \right), \quad (3.4e)$$

$$E_z^{n+1}(i,j,k+\frac{1}{2}) = E_z^n(i,j,k+\frac{1}{2}) + \frac{\Delta t}{\varepsilon \Delta x} \left(H_y^{n+\frac{1}{2}}(i+\frac{1}{2},j,k+\frac{1}{2}) - H_y^{n+\frac{1}{2}}(i-\frac{1}{2},j,k+\frac{1}{2}) \right)$$

$$+ \frac{\Delta t}{\varepsilon \Delta y} \left(H_x^{n+\frac{1}{2}}(i,j-\frac{1}{2},k+\frac{1}{2}) - H_x^{n+\frac{1}{2}}(i,J+\frac{1}{2},k+\frac{1}{2}) \right) , \qquad (3.4f)$$

The half time steps indicate that $\overline{E}$ and $\overline{H}$ fields are alternately calculated in order to achieve centered differences for the time derivatives. In these equations, the permittivity and the permeability are set to the appropriate values depending on the location of each field component. For the electric field components on the dielectric-air interface the average of the two permittivities $(\varepsilon_0 + \varepsilon_1)/2$, is used. The validity of this treatment is explained in [5].

Due to the use of centered differences in these approximations, the error is second order in both the space and time steps; i.e., if Δx, Δy, Δz and Δt are proportional to Δl, then the global error is $O(\Delta l^2)$. The maximum time step that may be used is limited by the stability restriction (discussed in section 4.2 chapter 4)of the finite difference equations,

$$\Delta t \leq \frac{1}{v_{\max}} \left(\frac{1}{\Delta x^2} + \frac{1}{\Delta y^2} + \frac{1}{\Delta z^2} \right)^{-1/2} , \qquad (3.5)$$

where v_{max} is the maximum velocity of light in the computational volume. Typically, v_{max} will be the velocity of light in free space unless the entire volume is filled with dielectric. These equations will allow the approximate solution of $\overline{E}(r,t)$ and $\overline{H}(r,t)$ in the volume of the computational domain or mesh; however, special consideration is required for the source, the conductors, and the mesh walls.

3.3 Excitation

The excitation pulse used in this investigation has been chosen to be Gaussian in shape. A Gaussian pulse has a smooth waveform in time, and its Fourier transform is also a Gaussian shape centered at zero frequency. These unique properties make it a perfect choice for investigating the frequency dependent characteristics of the NRD discontinuities.

An ideal Gaussian pulse which propagate with a velocity v in the $+z$ direction will have the following expression:

$$g(t, z) = \exp\left(-\frac{\left(t - t_o - \frac{z - z_o}{v}\right)^2}{T^2}\right) \quad , \quad (3.6)$$

where v is the velocity of the pulse in the specific medium, and the pulse has its maximum at $z = z_0$ when $t = t_0$ The Fourier transform of the above Gaussian pulse has the form

$$G(f) \propto \exp\left[-\pi^2 T^2 f^2\right] . \qquad (3.7)$$

The choices of the parameters T, t_0, and z_0 are subject to two requirements. The first is that after the space discretization interval Δx, Δy or Δz has been chosen fine enough to represent the smallest dimension of the structure The time discretization interval Δt has been chosen small enough to meet the stability criterion [2,5], the Gaussian pulse must be wide enough to contain enough space divisions for a good resolution. And at the same time the spectrum of the pulse must be wide enough (or the pulse must still be narrow enough) to maintain a substantial value within the frequency range of interest. If these last two conditions cannot be satisfied simultaneously, Δz has to be chosen even smaller. We define the pulse to be the width between the two symmetric points that have approximately 5 percent of the maximum value of the pulse. To determine T, suppose we define the pulse width to be the width between two points, which have 5 percent of the maximum value of the pulse. If W is the width of the pulse and is assumed to be 20 space steps wide, then T id determined from

$$\exp\left(-\frac{\left(\frac{W}{2}\right)^2}{(vT)^2}\right) = \exp(-3); (\approx 5\%) \qquad \text{or,}$$

$$T = \frac{1}{\sqrt{3}} \frac{10\Delta z}{v} .$$

By making this choice of T, the maximum frequency, which can be calculated, is

$$f_{max} = \frac{1}{2T} \; ; \qquad \left[G\!\left(\frac{1}{2T}\right) \approx 0.1 \right]$$

As long as the FDTD parameters satisfy the stability criteria described earlier, one can chose any convenient value for T. The second requirement is that the choice z_0 and t_0 be made such that initial "turn on" of the excitation will be small and smooth.

Another consideration in excitation is the specification of the spatial distribution of the field on the excitation plane. Ideally, the use of the dominant mode of distribution is preferred. But this distribution is generally not known with high enough accuracy. More the excitation is closer to the true field configuration, more faster is the convergence of the simulation.

3.4 Absorbing Boundary Conditions (ABCs)

A large number of electromagnetic problems have associated open space, where the spatial domain of the computational field is unbounded in one or more co-ordinate directions. The solution of such a problem in this form will require an unlimited amount of computer memory and processing time, which is impossible to arrange. Therefore, the domain must be truncated such that the error involved is minimal. For this, the domain can be divided into two regions: the interior region and the exterior region as shown in fig. 3.2. The interior region must be large enough to enclose the structure of interest. The exterior region is limited free space enclosing the interior region, and it simulates the infinite space. We apply the FDTD algorithm to the interior region. It simulates the wave propagation in the forward and backward directions. However, only outward

propagation in the exterior region is desired so that the infinite free space conditions are simulated.

Two options are available to simulate the open space surrounding the problem physical space: truncate the interior region with equivalent currents and use the Green's function to simulate the fields in the exterior region, to simulate the fields in the exterior region with absorbing boundary condition (ABCs) to minimize reflections from the truncation of the mesh [2]. In this thesis we adopted the ABC approach.

The absorbing boundary condition can be simulated in a number of ways. These are classified as analytical (or differential) ABC and material ABC. The material ABC holds great promise of truncating the mesh size. It can reach an ideal limit extending the FDTD numerical modeling capabilities to −80 to −120 dB reflection coefficient at the boundaries. Various types of absorbing boundary conditions are analyzed next.

EXTERIOR REGION

INTERIOR REGION

PROBLEM UNDER ANALYSIS
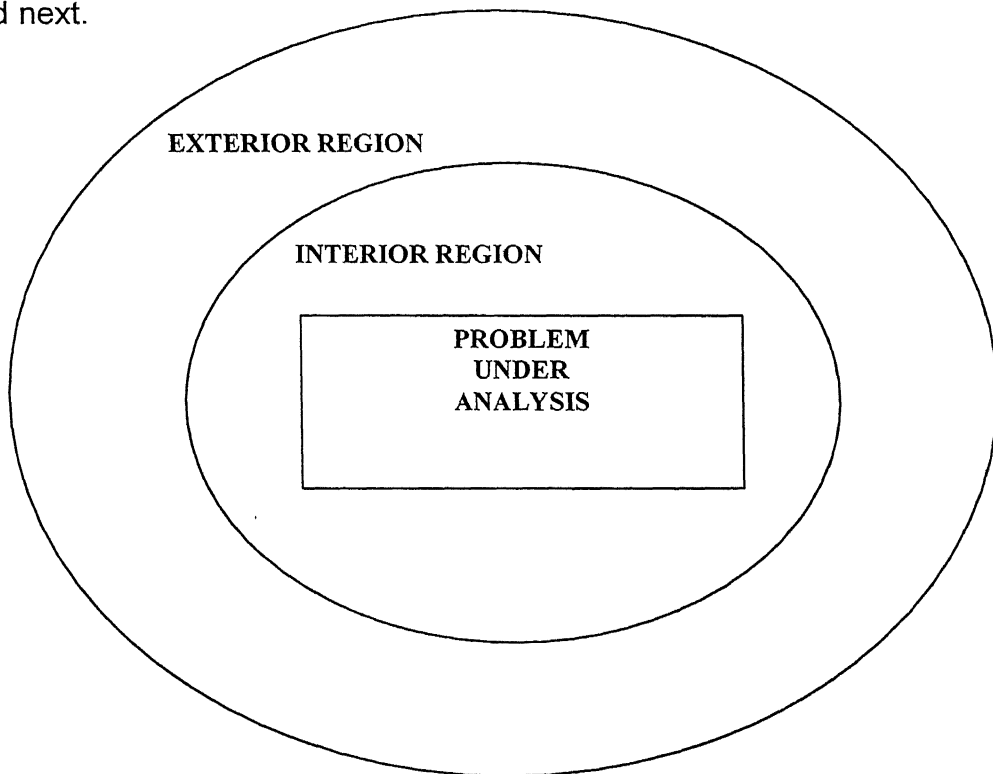
Fig. 3.2 Absorbing boundary conditions: an illustration

3.4.1 Analytical absorbing boundary conditions

Under this section the best and simple analytical ABC named Mur's first order absorbing boundary condition is selected to illustrate the basic principle underlying this type of ABCs.

Analysis for this absorbing boundary condition is based on the work of Enquist and Mazda [6], and the optimal implementation was given by Mur [7]. An arbitrary wave can be expanded in terms of a spectrum of plane waves. If a plane wave is normally incident on a plane surface, and the surface is perfectly absorbing, there will be no reflected wave. Consider the following differential equation,

$$\left(\frac{\partial}{\partial x} - \frac{1}{c} \frac{\partial}{\partial t} \right) \phi\,(x,t) = 0, \tag{3.8}$$

The solution of the above equation can be easily written as $f(x+ct)$, a left traveling wave i.e., zero reflection coefficient is obtained in this case. Therefore (3.8) can be used to determine the absorbing condition for a normally incident wave. For updation of electric field at $x = \Delta x/2$, $t = (n+1)\Delta t$, we have to discretize the following expression

$$\frac{\partial \phi(x,t)}{\partial x} = \frac{1}{c} \frac{\partial \phi(x,t)}{\partial t} \Bigg|_{x=\frac{\Delta x}{2}, t=(n+\frac{1}{2})\Delta t} . \tag{3.9}$$

In finite difference form, equation (3.8) can be written as

$$\frac{\phi_1^{\,n+1/2} - \phi_0^{\,n+1/2}}{\Delta x} = \frac{1}{c} \frac{\phi_{1/2}^{\,n+1} - \phi_{1/2}^{\,n}}{\Delta t} \tag{3.10}$$

In this form finite difference approximation is accurate to second order in Δx and Δt. But the values at the half grid points and half time steps are not available, and can be averaged as,

$$\phi_m^{\,n+1/2} = \frac{\phi_m^{\,n+1} - \phi_m^{\,n}}{2} \tag{3.11a}$$

and

$$\phi_{m+1/2}^{n} = \frac{\phi_{m+1}^{n} + \phi_{m}^{n}}{2} \quad , \tag{3.11b}$$

The approximation of (3.11) is also accurate to a second order if $\Phi(x,t)$ is a smooth function. Use of (3.11) in (3.10) yields,

$$\phi_{0}^{n+1} = \phi_{1}^{n} + \left(\frac{c\Delta t - \Delta x}{c\Delta t + \Delta x}\right)\left(\phi_{1}^{n+1} - \phi_{0}^{n}\right). \tag{3.12}$$

This is the equation for updating the fields, which are lying on the outer boundary. Equation (3.12) can be shown to be unconditionally stable [7]. The boundary condition (3.8) is exact only for a plane wave at normal incidence. Hence the wave will be reflected for an oblique incidence. To take care of this eventuality one needs to use higher order absorbing boundary condition.

Based on the above procedure we can derive the ABCs for the $\overline{E}$ field components at the boundaries of x, y and z axes by substituting ϕ in the above equations by $\overline{E}$ or $\overline{H}$ whichever applicable.

3.5 Extraction of frequency domain characteristics from the time-domain data.

The FDTD has been used extensively for calculating the frequency domain characteristics such as voltage or current distributions, propagation constant, S-parameters and driving point impedance, etc. When the frequency response over a broad spectrum is of interest, a broadband pulse excitation can provide this frequency response with a single FDTD simulation. The conversion from the time domain to frequency domain is achieved using either a Discrete Fourier Transform (DFT) or a Fast Fourier Transform (FFT). Using DFT, transformation from time domain to frequency domain is described as,

$$G(x,y,z,t) = \Delta t \sum_{n=0}^{N-1} g(x,y,z,n\Delta t)\exp(-j2\pi f n\Delta t) \quad , \tag{3.13}$$

36

where g(*x,y,z,nΔt*) is the pulse response, Δt is the sampling interval, and N is the total number of samples.

The determination of characteristics like resonant frequency and S-parameters from the pulse response is described next.

3.5.1 Resonant frequency

To determine the resonant frequency of a cavity, we should select an appropriate field component in the stabilized mode pattern. Next, the positions of the peak amplitude in the frequency spectrum are defined. These positions provide the resonant frequencies of the various modes excited in the structure under consideration. However, these modes can be identified if one plots the field distribution inside the cavity at these resonant frequencies.

3.5.2 S-parameters

In addition to the transient results obtained naturally by the FDTD method, the frequency-dependent scattering matrix coefficients are calculated.

$$[b]=[S][a] \quad ,$$

(3.14)

where $[b]$ and $[a]$ are proportional to the reflected and incident voltage vectors, respectively, and $[S]$ is the scattering matrix. Where

$$a = \frac{v^+}{\sqrt{z_0}} \quad ,$$

(3.15)

and

$$b = \frac{v^-}{\sqrt{z_0}} \quad .$$

(3.16)

To accomplish this first the electric field at each port is recorded first. As in [5] and [10], it is assumed that this field value is proportional to the voltage (which could be obtained by numerically integrating the vertical electric field) when considering propagation of the fundamental mode. To obtain the scattering

parameter $S_{11}(\omega)$, the incident and reflected voltages must be known. The FDTD simulation calculates the sum of incident and reflected voltages. To obtain the incident waveform, the calculation is performed using only the port1 of the NRD guide which will now be of infinite extent (from source to far absorbing wall), and the incident waveform is recorded. This incident waveform may now be subtracted from the incident plus the reflected wave for port 1. The scattering parameters, S_{jk}, may then be obtained by FFT of these transient waveforms as

$$S_{jk}(\omega) = \frac{FFT\{V_j(t)\}}{FFT\{V_k(t)\}}$$
(3.17)

The reference planes are chosen sufficiently far from the circuit discontinuities so that evanescent waves have decayed to a very small value.

3.6 Algorithm

So far in the chapter, we dealt with the various aspects of the FDTD technique. When it is applied to a particular problem, a sequential procedure need to be followed which is illustrated as a flow chart in figure 3.3. From fig. 3.1 one can see that the electric and magnetic fields in a Yee's cell are separated by half-a- step in space. So as the case with respect to time. That is, after the electric fields on the grid have been calculated, time is increased by half-a- step and then the magnetic fields are updated. Similarly the positions of the magnetic fields are half space step away from the corresponding electric field components.

```
                    ┌─────────────┐
                    │    START    │
                    └─────────────┘
                           │
                           ▼
            ┌──────────────────────────────┐
            │ DEFINE      PHYSICAL       &  │
            │ MATERIAL  CONSTANTS  OF       │
            │ THE PROBLEM                   │
            └──────────────────────────────┘
                           │
                           ▼
            ┌──────────────────────────────┐
            │ CALCULATE    THE    SPACE     │
            │ AND TIME INCREMENTS           │
            └──────────────────────────────┘
                           │
                           ▼
            ┌──────────────────────────────┐
            │ SET THE BOUNDARY CONDITIONS   │
            │ GLOBALLY  AND  INITIALIZE THE │
            │ FIELDS                        │
            └──────────────────────────────┘
                           │
                           ▼
            ┌──────────────────────────────┐
            │     SOURCE EXCITATION         │
            └──────────────────────────────┘
                           │
                           ▼
            ┌──────────────────────────────┐
            │ UPDATE  THE  H-FIELD  AND  E- │
            │ FIELD   COMPONENTS   ON  THE  │
            │ WHOLE DOMAIN AND SAVE         │
            └──────────────────────────────┘
                           │
                           ▼
            ┌──────────────────────────────┐
            │      IMPLEMENT ABCs           │
            └──────────────────────────────┘
                           │
                           ▼
                        ( @ )
```
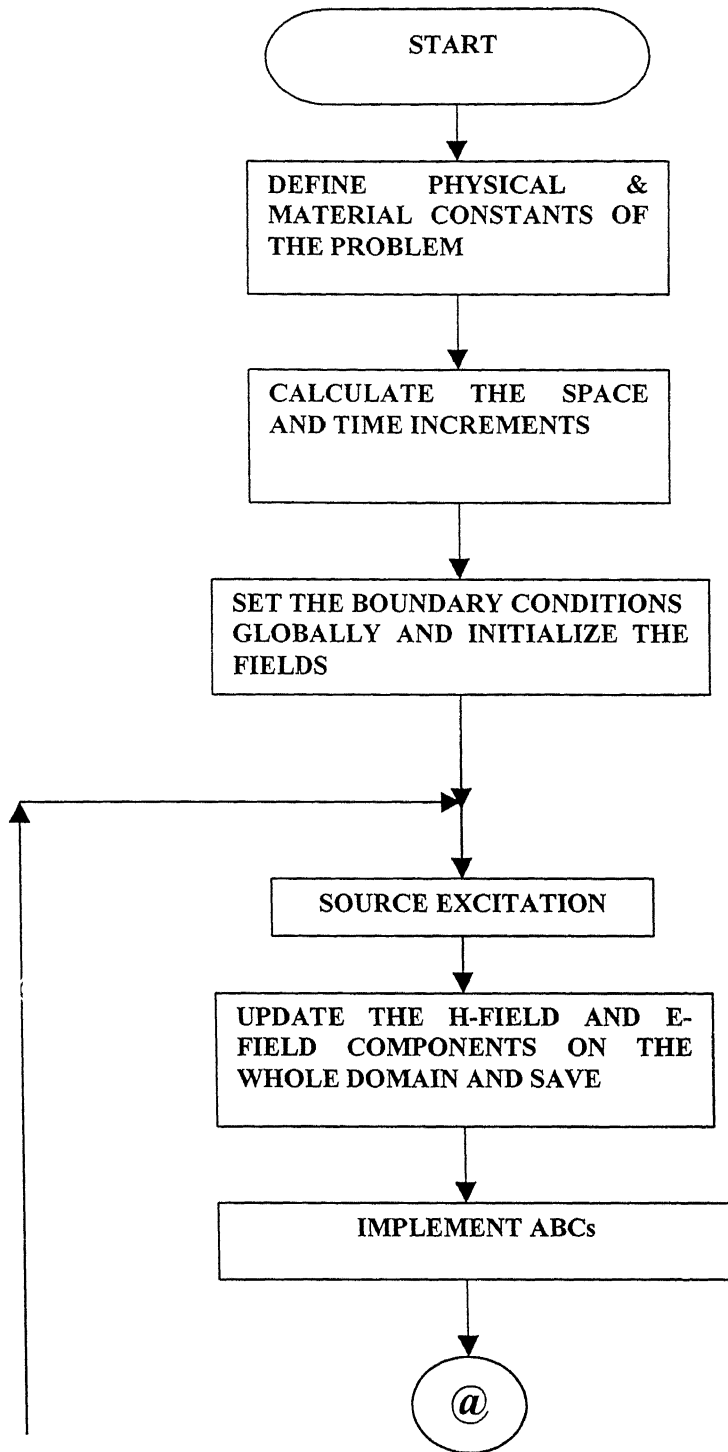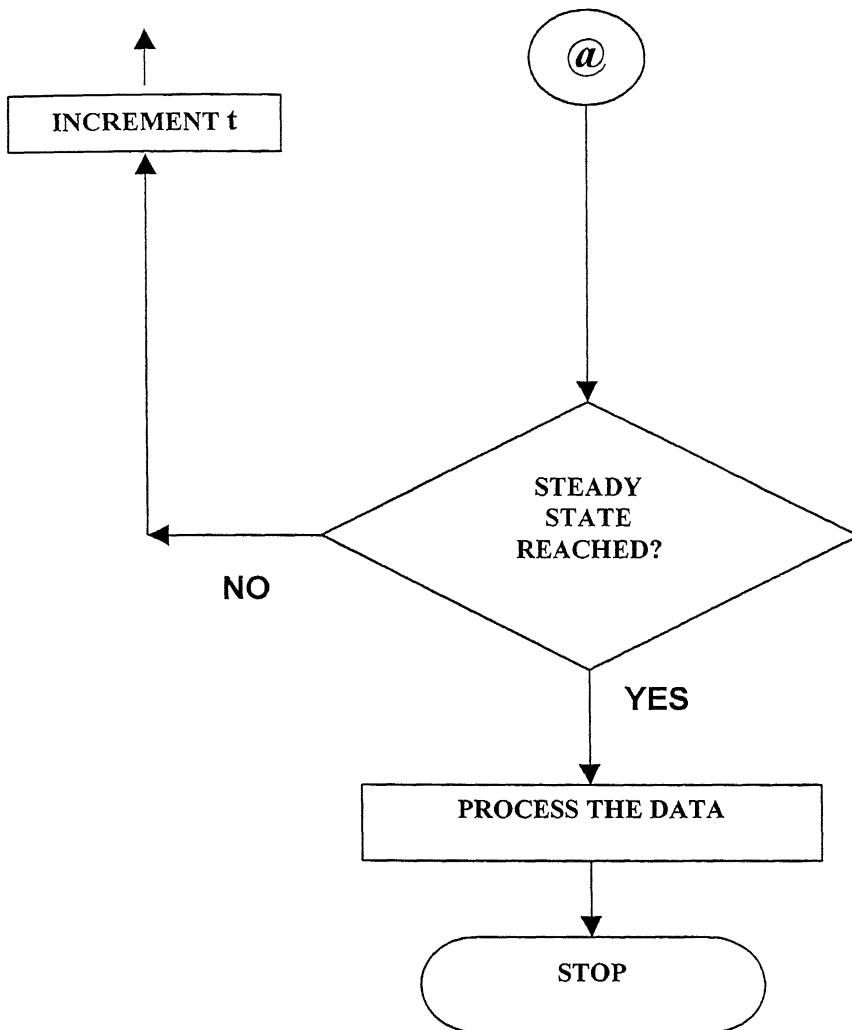
Fig. 3.3 Flow –chart for FDTD formulation.

3.7 Coding

All the coding for our simulation has been done in MATLAB environment. The is divided into the following categories:

- *Constant declaration:* All the physical parameters associated with the FDTD simulation such as the velocity of light, electric permittivity, magnetic permeability, and the dielectric constant of the medium are defined.

- *Field initialization:* A "Structure" (A data-structure used in programming languages) which has six real quantities associated with it has been used us. The six quantities stand for the six field components (E_x, E_y, E_z and H_x, H_y, H_z) One such structure is associated with each Yee's cell. So one needs an array of such structures to accommodate the whole grid. Before the simulation starts, all the field components inside the grid are initialized to zero.

- *Excitation:* In the excitation part we impinge an electric field source on a chosen plane.

- *Field updation:* After the field excitation has been carried out, the magnetic and the electric fields in each "structure" of the grid are modified.

- *Saving and processing:* In this part, the field data at the required planes is stored at each time step. All the time-domain data stored is then processed to get either a real time field display or frequency-domain parameters.

The above description gives an outline of the code. The actual code, however, has lot of conditional statements and control loops which are necessary to check conditions and for looping etc.

Chapter 4

Results and Discussion

4.1 Introduction

Based on the FDTD principles described in chapter 3, we have developed a code, which can be applied to two and three-dimensional electromagnetic structures. The source code was written in MATLAB environment. In some cases one is interested only in the field behavior inside the structure in real time rather than the frequency domain results. An example is the measurement of Specific Absorption Rate (SAR) of the complex tissue of a human head due to exposure to the radiation from a typical 1900 MHz. Cellular phone. FDTD measured results with visualization are a powerful tool in this case [2]. In majority of the electromagnetic systems, it is the frequency-domain data that has more importance and relevance. Fourier transforming the time-domain response gives the frequency-domain results.

4.2 Testing of the code

The first logical step after software has been written is to test it for known cases. Published results are not available for NRD guide discontinuities and the number of papers available in this area are also very few. The best way to ascertain the proper functioning of the code is to test it for an EM structure whose behavior known. For this purpose we have chosen the problem given in the famous paper on FDTD by its discoverer Yee [1], with small changes. Consider

the diffraction of an incident TM wave by a perfectly conducting square. The geometry of the problem along with the dimensions is shown in figure 4.1.

The input is a Z-directed electric field source excited on the line shown. Source distribution is selected as Gaussian and the width of the pulse is taken narrow enough to have a wide bandwidth of operation. The FDTD parameters used for the computation are given in Table 4.1.

Except on the source line, all other field components on the grid are evaluated through FDTD expressions for the field components

The code was first executed without the conducting square obstacle inside structure. The observation period was about 250 time steps. The resulting electric field distribution was sampled at different times on the whole domain. Figure 4.2 shows the electric field on the line j=50 for i = 1 to 100 at different time instants without the square obstacle. Next, the perfectly conducting square obstacle has been placed as in the original problem and the FDTD routine was repeated. Figure 4.3 shows the electric field on the same line at different time instants. The results obtained by Yee are shown in figure 4.4. Note that Yee has given the excitation from left to right on the right side of the obstacle, whereas we have adopted a more general convention of left to right excitation on the line j=1. The electric field distribution on the whole grid sampled after 15,90 and 120 time steps is shown in figures 4.5 through 4.7 respectively.
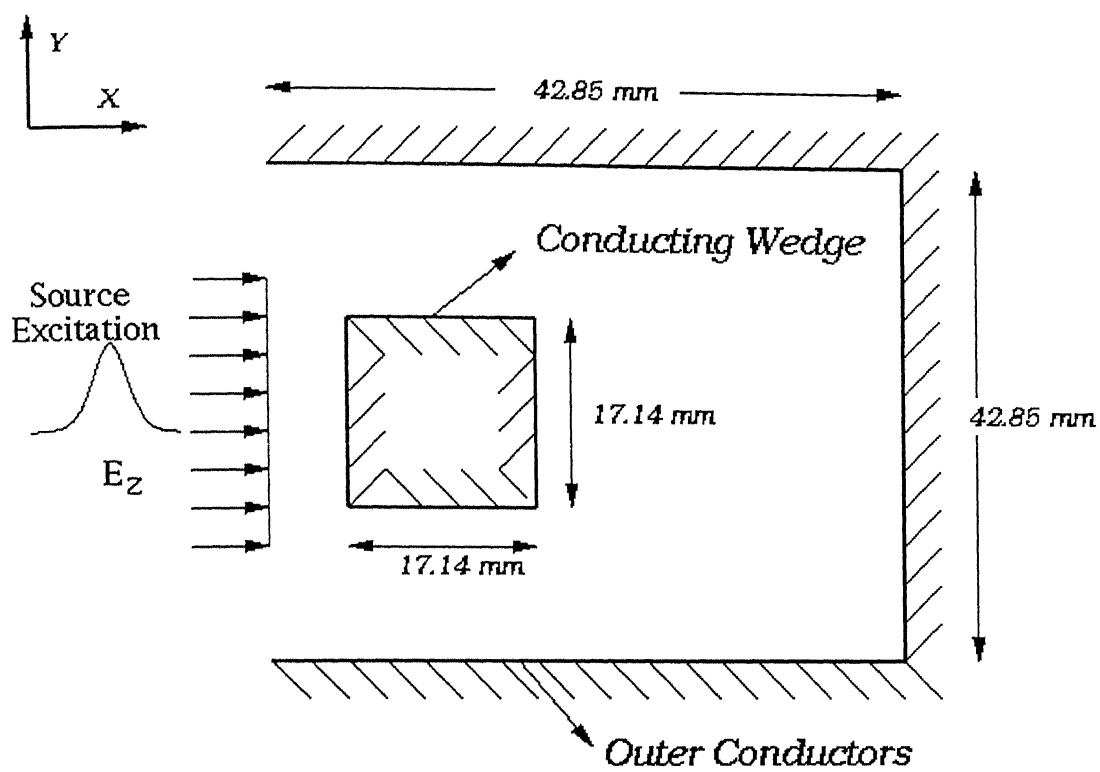
Fig. 4.1 Yee's problem

Table 4.1 FDTD parameters for the Yee's problem

| S. No.	FDTD Parameter	Symbol	Numerical Value
1	Velocity of EM wave in free space	C	299792458 m/s
2	Permeability	μ_0	$4\pi \times 10^{-7}$ henry/m
3	Permittivity of free space	ε_0	8.854×10^{-12} F/m
4	Frequency	f_c	35 GHz
5	Space step in Yee's cell	Δ	0.43 mm
6	Time step	Δt	1.01 ps
7	Length	A	42.86 mm
8	Breadth	B	42 86 mm
9	Dimension of square obstacle	L	17.14 mm
10	No. of cells along length (X-dir.)	n_x	100
11	No. of cells along breadth (Y-dir.)	n_y	100
12	Source excitation (Gaussian in space and time) [Electric, Z-directed TM wave].	S_0	$E_0 e^{\left(-\left(\frac{t-16\Delta t}{4\Delta t}\right)^2\right)}$ $(E_0 = 1)$
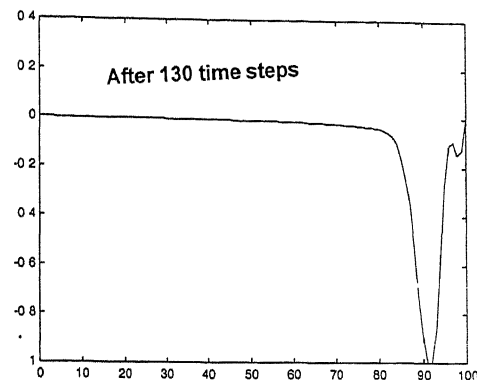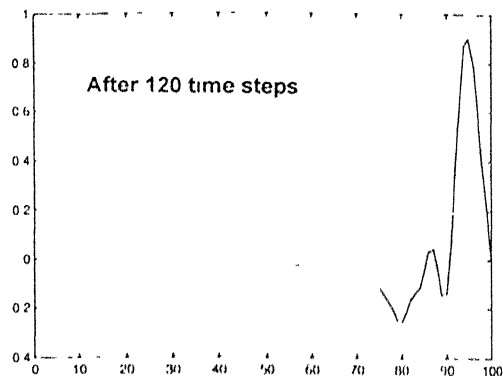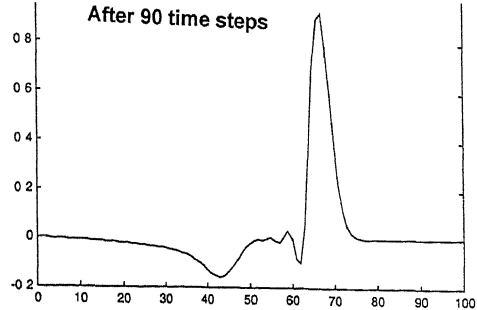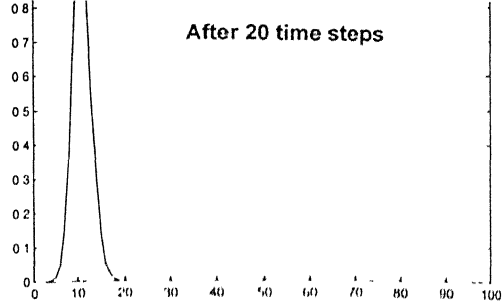
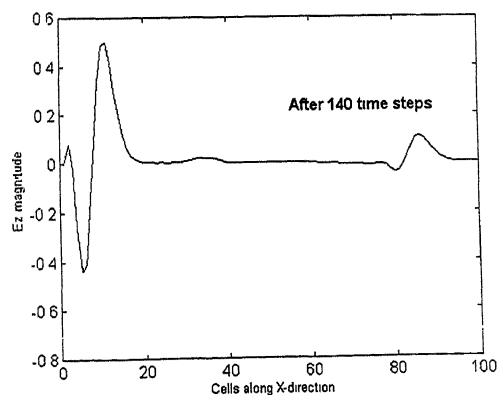**Fig. 4.2** E_z on the line y=50 at various time instants on the grid without the obstacle.
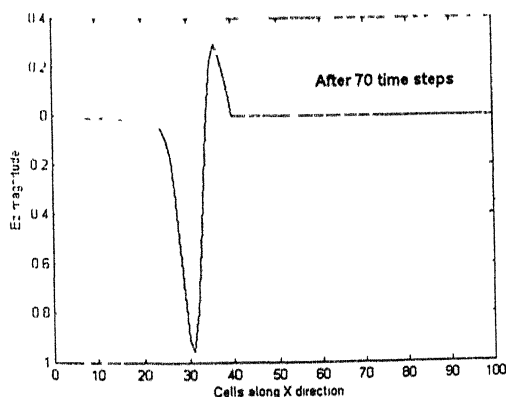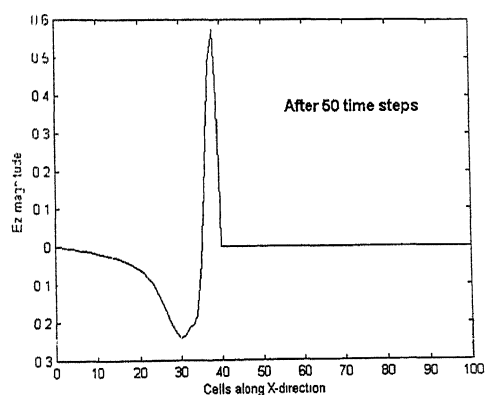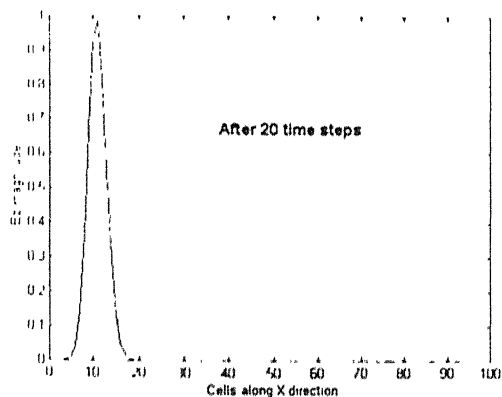

Fig. 4.3 E_z on y=50 line with the obstacle
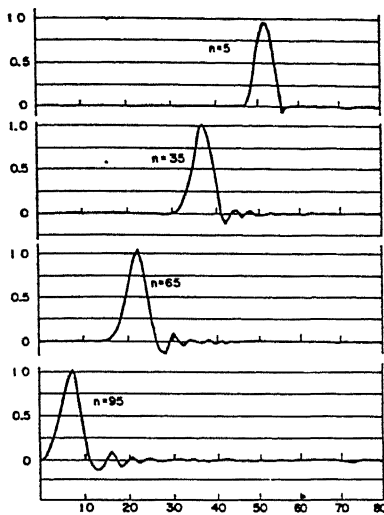
g 3 Results of the calculation of E_s by means of (14a)–(14c) in the absence of the obstacle The ordinate is in volts/meter and the abscissa is the number of horizontal increments *n* is the number of time cycles.
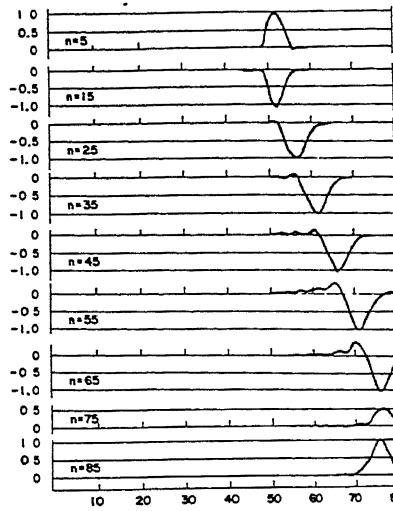
Fig 5. E_s of the TM wave for various time cycles $j = 50$

Fig. 4.4 Yee's results [Note that the excitation in this case is from right to left

Ez on the 100 X 100 grid sampled after 15 time steps

Fig. 4.5 Electric field distribution on the grid sampled after 15 time steps in the simulation.
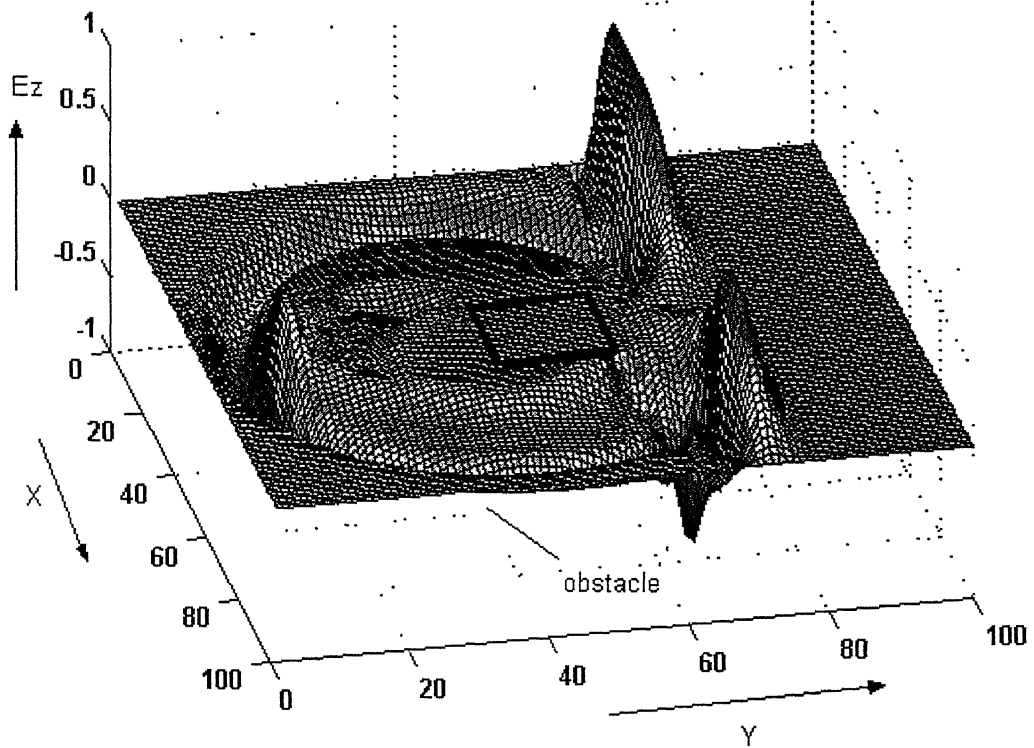
Fig. 4.6 Electric field sample on the grid after 90 time steps.
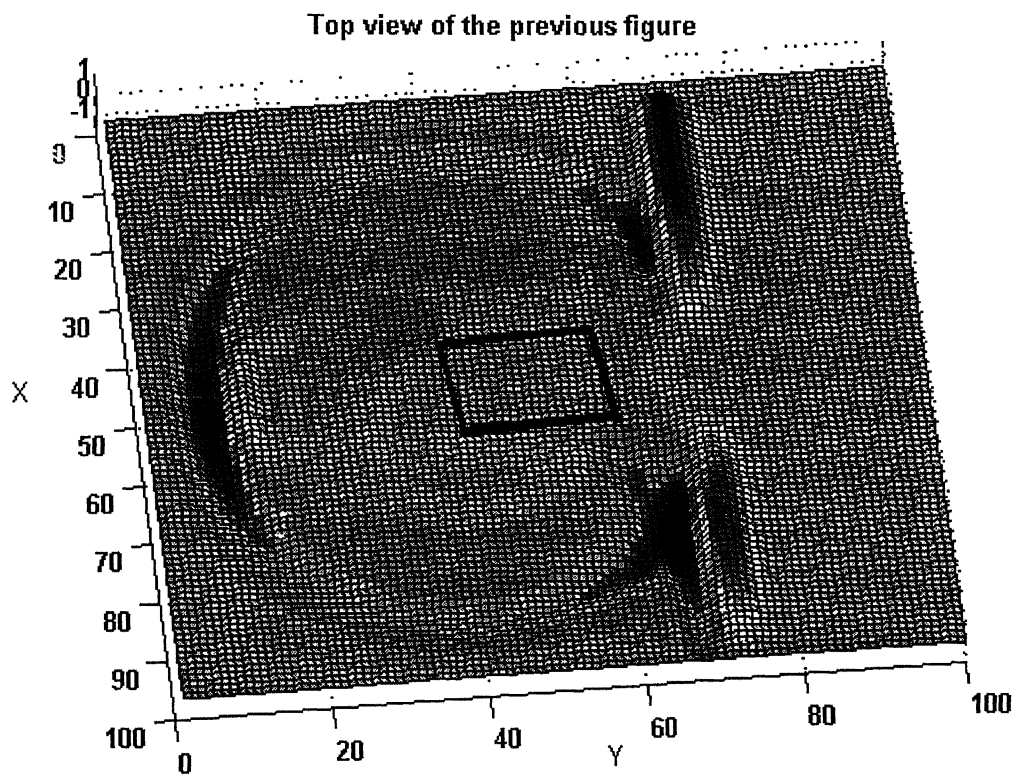
Fig. 4.7 Top-view of the previous figure
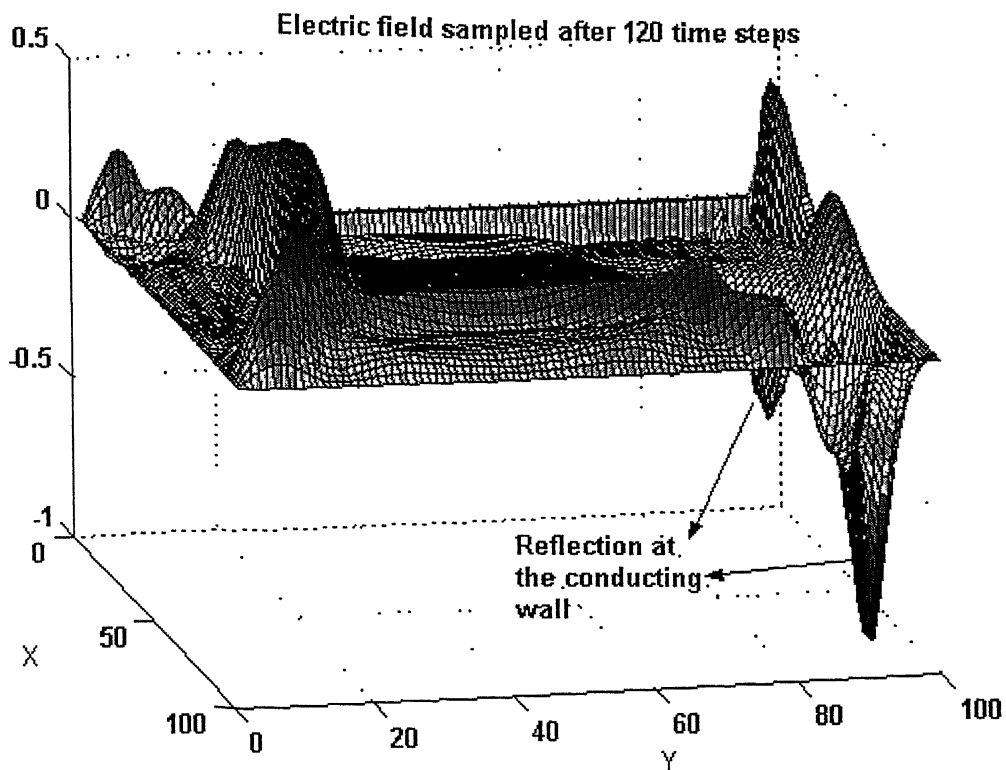
4.8 Electric field on the grid sampled after 120 time steps

Comparing the results obtained by Yee shown in figure 4.4 with our resulrs shown in figures 4.2, 4.3 and 4.5 through 4.8, we see that they do not match perfectly. There may be several reasons for this:
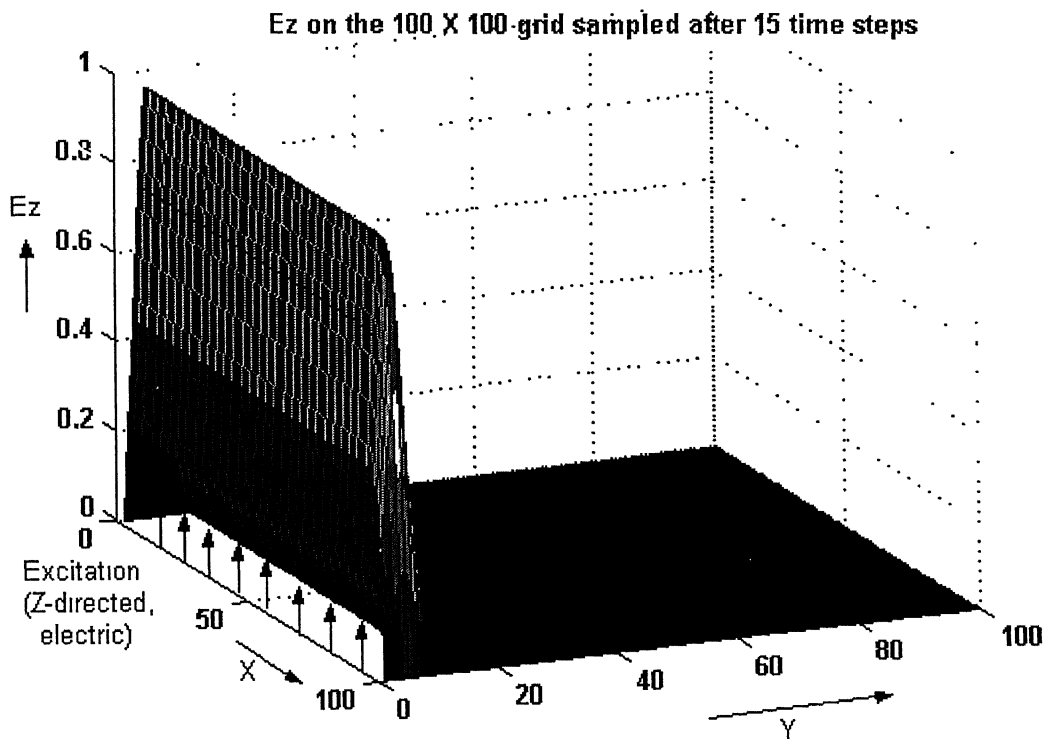
- *The excitation:* The excitation used by Yee was half-sinusoidal with shape similar to a Gaussian pulse whereas we have used a pure Gaussian pulse.

- *The FDTD parameters:* Our actual code was to be applied for NRD guides. Keeping that in view we have chosen the FDTD parameters such as space and time steps. These differ from those of Yee.

The reason for simplifying the original problem is that primarily we wanted to test our code for two crucial factors:

1. **Stability of the simulation:** As stated, we carried out the simulation for 250 time steps. At each time step we update the electric and magnetic fields on all the 10,000 Yee's cells. The field values at each time step in every cell depend on the values of the fields at previous time step in the cell as well as the fields

in the adjacent cells. Due to the huge number of iterations involved, the error accumulates rapidly. To see this, define stability factor as,

$$S = \frac{c\Delta t}{\Delta},$$

(4.1)

where c is the velocity of electromagnetic radiation in free space , Δt and Δ are time and space increments respectively. As long as $S \leq 1$, the simulation will be stable [2]. If $S > 1$, even by a small percentage, the error will accumulate rapidly and soon the solution will "blow up". We used $S = 0.7$ in our simulation. Figure 4.9 is the E_z field plot on y=50 on the grid after 90 time steps (reproduced from fig. 4.2) with $S=0.7$. The same plot with s=1.2 is shown in figure 4.10. The oscillatory behavior is clearly seen. The magnitude has also risen to a staggering 10^{95} ! This indicates how sensitive the FDTD simulation stability with respect to the stability factor S. Therefore extreme care must be taken while choosing Δt and Δ.
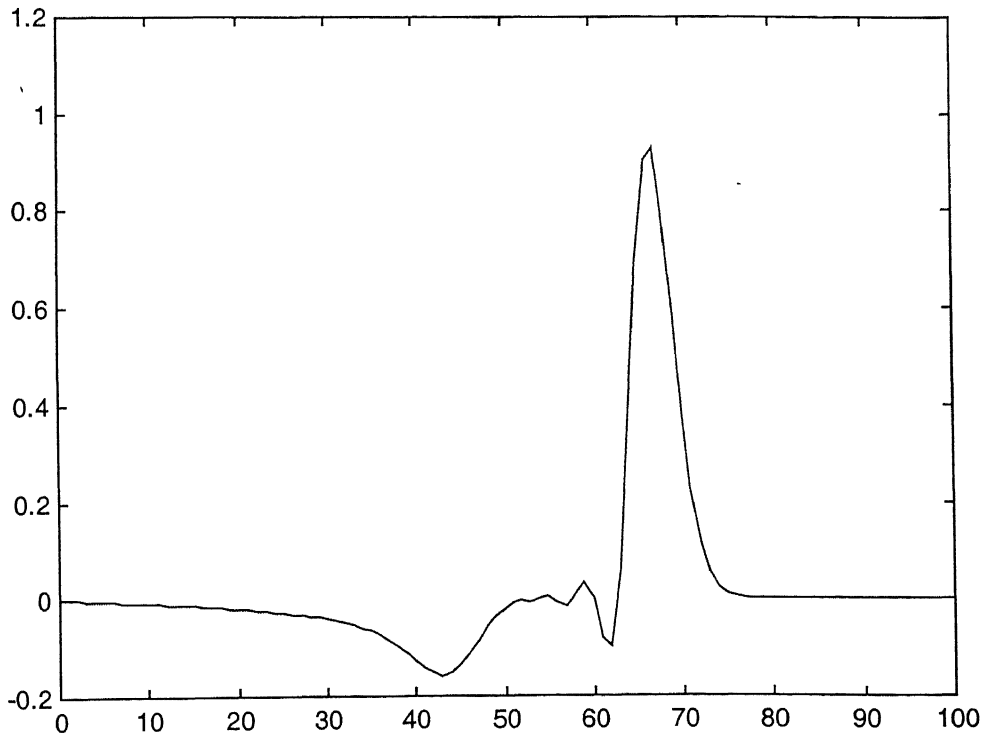
Fig. 4.9 E_z magnitude on y=50 with stability factor $S=0.7$
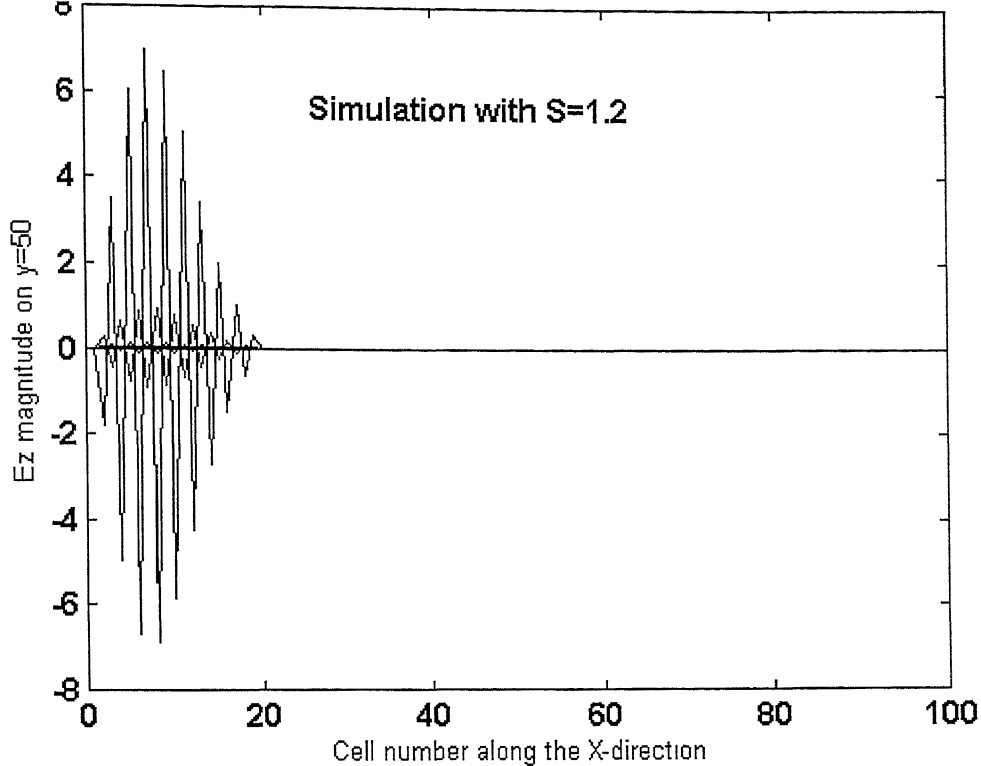
Fig. 4.10 Result of the simulation of the same problem, but with S=1.2

2. **Propagation of the numerically calculated wave:** After launching the pulse into the structure, we calculate the fields on the grid through FDTD expressions. A correct simulation will show the wave or pulse "propagating", as the time passes by. This is evident from figures 4.2 through 4.8.

3. **Behavior at the conducting boundaries:** The knowledge given to the code before the simulation is performed is, the expressions for the discretized Maxwell's equations, the setting of the tangential electric fields on the conducting boundaries to zero and the geometry of the structure under analysis. A correctly formulated code should result in the phase reversal of the numerically calculated wave at the conducting boundaries. Our code has functioned as expected in this front. This is evident from figures 4.6 and 4.7, which show the diffraction at the conducting square very clearly.

Having tested the code for all the crucial aspects of FDTD technique described above, we applied it to NRD discontinuities described hereafter.

51

4.3 NRD guide discontinuities

We applied the FDTD technique to three NRD guide discontinuities namely open-end, end coupled gap discontinuity and the edge coupled gap discontinuity. In all the three cases the frequency of interest was 35 GHz. The aim was to obtain the frequency dependent scattering parameters for each discontinuity.

4.3.1 Processing the Time-Domain results

The computational was carried for approximately 450 time steps for each discontinuity storing the desired field components at each time step. After each time step, we store the desired electric field components on each Yee's cell on the input and the output planes at sufficient distance from the discontinuity. The corresponding voltages are obtained through numerical integration. Next, the S-parameters were calculated as per the procedure discussed in chapter 3.

The Mur's ABCs described in chapter 3 are used in our simulation. While the excitation is given at one of the ports, the power coming out at the other port needs to be absorbed to simulate a matched load condition.

4.4 Open-end NRD guide discontinuity

The open-end NRD guide discontinuity is shown in figures 2.4 and 2.5 of chapter 2. The source excitation is carried out at the front face. Table 4.2 gives all the FDTD parameters used for the computation.

The magnitude and the phase of S_{11} are shown in figures 4.11 and 4.12 respectively. As can be seen from figure 4.11, the magnitude of the reflection coefficient S_{11} is close unity indicating that most of the power is reflected back at the discontinuity. Note that the conducting plates that confine the NRD guide at the top and bottom are continued even after the abrupt termination of the dielectric strip, to reduce the losses due to radiation.

Table 4.2 FDTD parameters for open-end discontinuity

| S. No.	FDTD Parameter	Symbol	Numerical Value
1	Velocity of EM wave in free space	C	299792458 m/s
2	Permeability	μ_0	$4\pi \times 10^{-7}$ henry/m
3	Permittivity of free space	ε_0	8.854×10^{-12} F/m
4	Relative Dielectric constant (Alumina)	ε_r	9.5
5	Frequency	f_c	35 GHz.
6	Space step in Yee's cell	Δ	0.43 mm
7	Time step	Δt	0.2678 ps
8	Width	a	3.86 mm
9	Thickness	b	1.32 mm
10	Dielectric strip length	m	4.29 mm
11	Width of the front face	w	3.00 mm
12	Length	l	8.57 mm
13	No. of cells along width (Z-dir.)	n_z	9
14	No. of cells along thickness (Y-dir.)	n_y	7
15	No. of cells along length (X-dir.)	n_x	20
16	Source excitation (Gaussian in space and time) [Electric]	S_0	$E_0 e^{\left(-\left(\frac{t-20\Delta t}{10\Delta t}\right)^2\right)}$ $(E_0 = 1)$
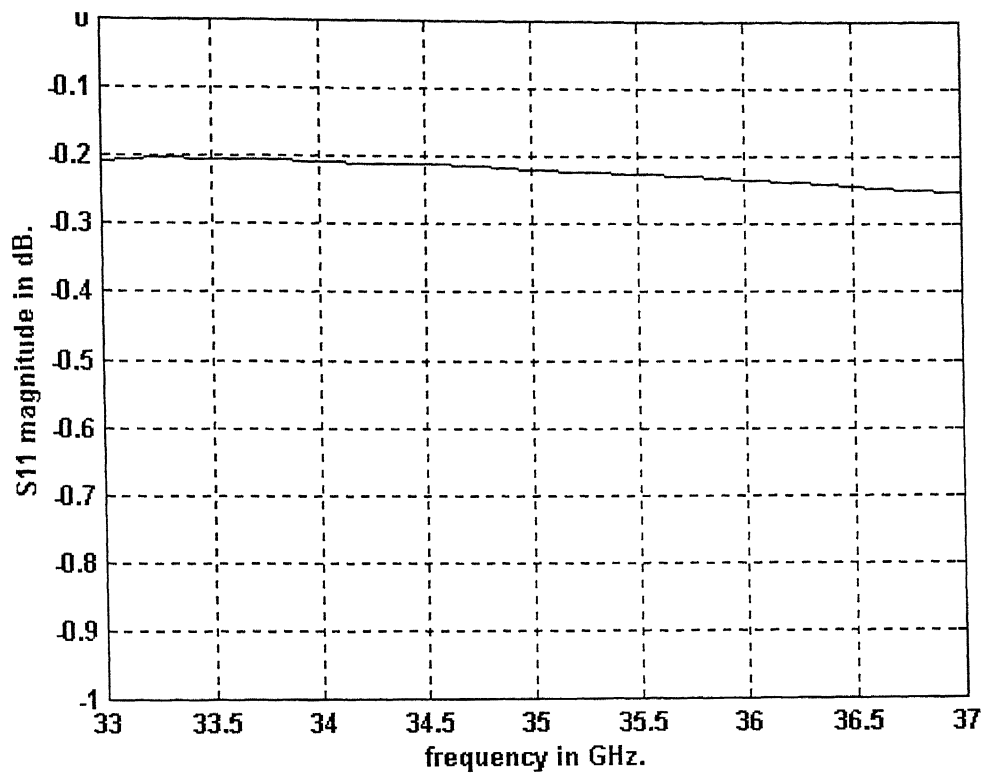
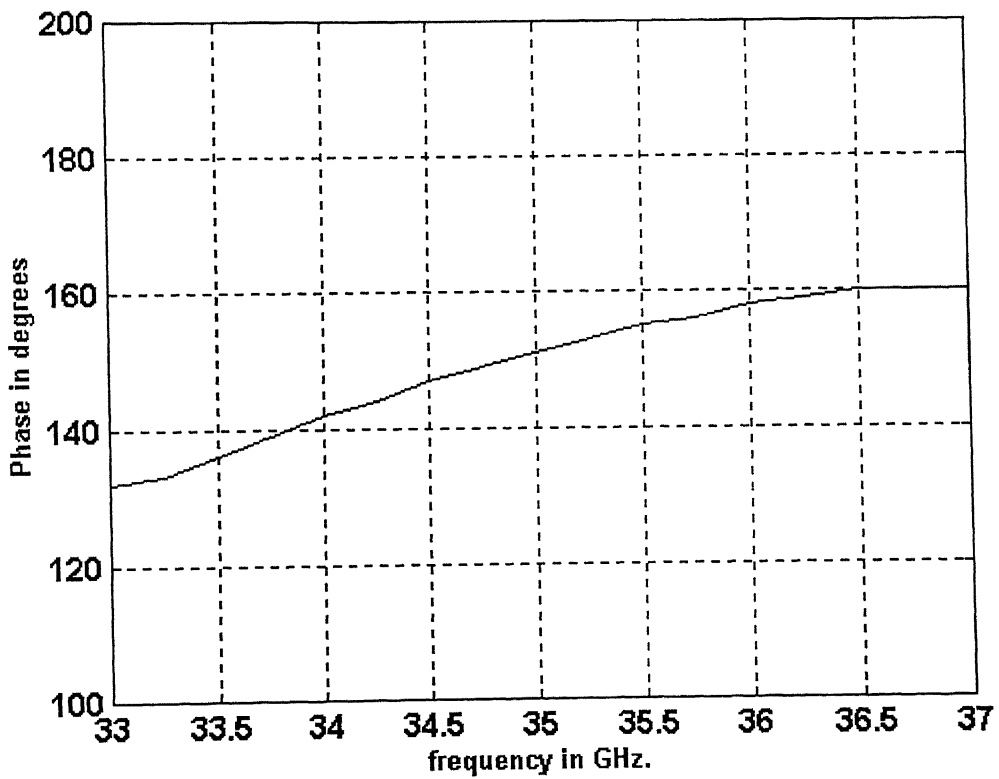**Fig. 4.11** Magnitude of reflection coefft. Versus frequency for open-end.

Fig. 4.12 Phase of S_{11} versus frequency for open-end

4.5 End-coupled gap discontinuity

We consider next the analysis of NRD guide based end-coupled gap discontinuity, where there is an air-gap in the dielectric strip along its length. We had FDTD simulated the structure for two different gaps of 0.86mm and 1.72 mm at 35 GHz. center frequency. The structure we are considering is symmetric along the length.

4.5.1 End-coupled gap discontinuity with 0.86mm gap.

The end-coupled NRD guide discontinuity is shown in figures 2.6 and 2.7. The FDTD analysis is carried out in the same manner as the earlier one. The FDTD parameters are given in table 4.3. The Mur's Absorbing Boundary Conditions are simulated at the output port.

The magnitudes of the frequency dependent scattering parameters S_{11} and S_{12} are shown in figure 4.13, and the corresponding phases in figure 4.14. From figure 4.13 we observe that the scattering coefficient S_{11} is around -0.7 dB. at 35 GHz. As the frequency is increased from 33 GHz. to 37 GHz., the reflected power is decreased due to the coupling effect. Increase in the coupled power is seen from the plot of the scattering parameter S_{12}.

From the scattering parameters one can also obtain the equivalent T or a Π network of the discontinuity. In general, it is desirable that in an equivalent circuit, the constituent impedance values are also given as a function of frequency. To achieve this, the simulation need to be carried out for a large number gap widths in a range of interest and the equivalent impedance parameters for each run is to be calculated. To this data one can fit a curve using interpolation techniques, obtaining the required design curves. In the present work, we analysed each discontinuity for two different gap widths which is not enough to obtain the design curves. Therefore we did not attempt the equivalent circuits.

Table 4.3 FDTD parameters for end -coupled gap discontinuity with 0.86 mm gap.

S. No.	FDTD Parameter	Symbol	Numerical Value
1	Velocity of EM wave in free space	C	299792458 m/s
2	Permeability	μ_0	$4\pi \times 10^{-7}$ henry/m
3	Permittivity of free space	ε_0	8.854×10^{-12} F/m
4	Relative Dielectric constant (Alumina)	ε_r	9.5
5	Frequency	f_c	35 GHz.
6	Space step in Yee's cell	Δ	0.43 mm
7	Time step	Δt	0.2678 ps
8	Width	a	3.86 mm
9	Thickness	b	1.32 mm
10	Length	l	9.43 mm
11	Length of each dielectric strip	m	4.29 mm
12	Width of the front face	w	3.00 mm
13	Gap width	p	0.86 mm
14	No. of cells along width (Z-dir.)	n_z	9
15	No. of cells along thickness (Y-dir.)	n_y	7
16	No. of cells along length (X-dir.)	n_x	22
17	Source excitation (Gaussian in space and time) [Electric]	S_0	$E_0 e^{\left(-\left(\frac{t-20\Delta t}{10\Delta t}\right)^2\right)}$ $(E_0 = 1)$

4.13 Magnitudes of reflection and transmission coefficients of an NRD end-coupled guide with 0.86 mm gap.
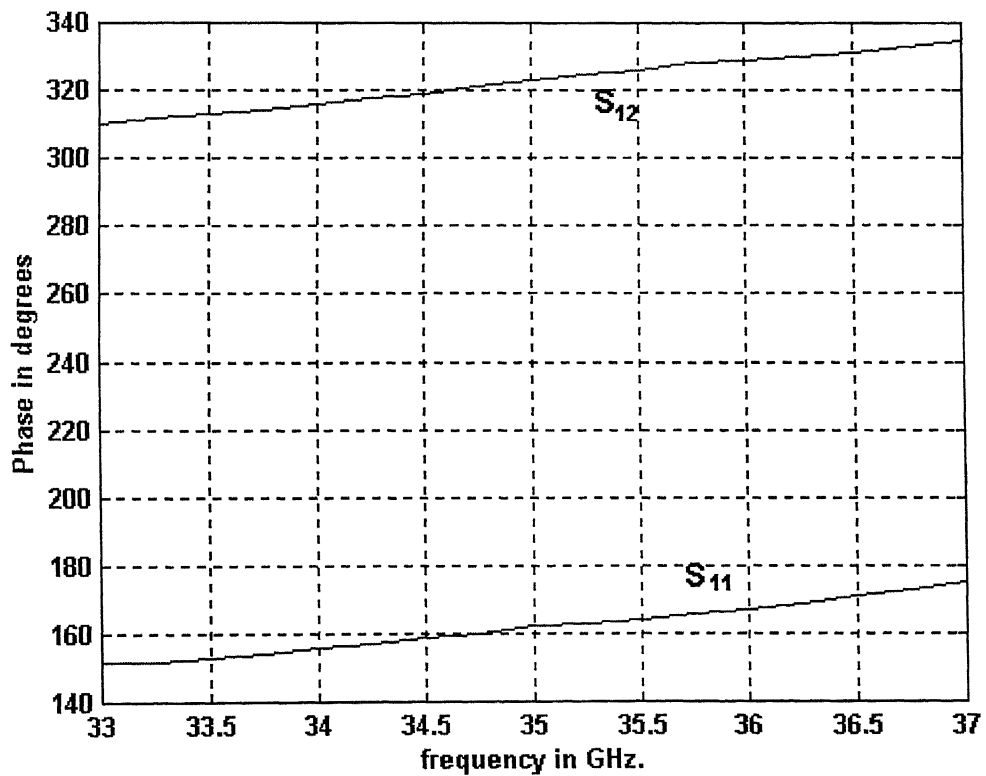
4.14 Phase versus frequency of S_{11} and S_{12} of 0.86 mm gap coupled NRD guide

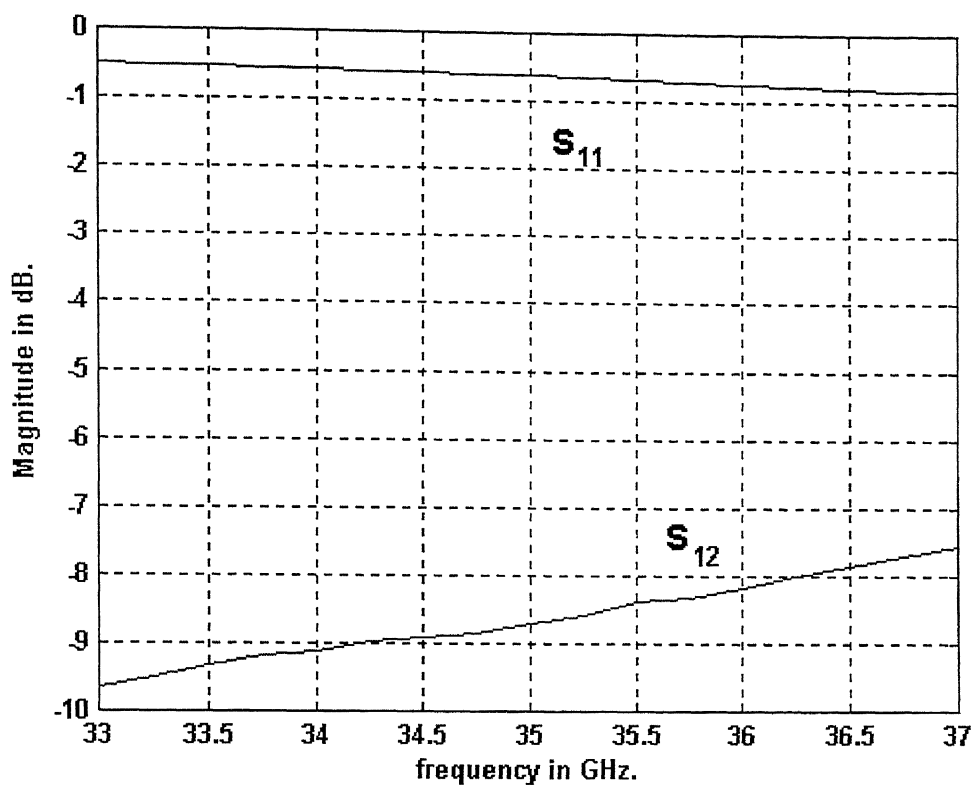## 4.5.2 End-coupled gap discontinuity with 1.72 mm gap.

The end-coupled NRD guide discontinuity is shown in figures 2.6 and 2.7. The FDTD analysis is carried out in the same manner as the earlier one. The FDTD parameters are given in table 4.4. The magnitudes of the frequency dependent scattering coefficients S_{11} and S_{12} are shown in figure 4.15 and the corresponding phases in fig. 4.16.

It can be observed from the figure 4 15 that, as the coupling gap is increased, the discontinuity starts behaving like an open end. The reason is, with increasing gap length, the coupling becomes ineffective as the fields outside the dielectric strip decay rapidly at little distances. Also there is a gradual rise in the coupled power with the frequency. The phases of both S_{11} and S_{12} have shown an increase with increasing frequency.

4.6 Edge-coupled NRD guide discontinuities

We have seen that in end coupling there is a gap between the dielectric strips along the length of the NRD guide. In edge coupled NRD guides, the coupling is between the strips which are placed side by side with a small separation. Here the coupling length is defined as the width of intersection between the two dielectric strips placed side by side. In the subsequent sections we have described our analysis of the edge-coupled NRD guide discontinuities with two different coupling lengths namely 0.43 mm and 0.86 mm

4.6.1 Edge-coupled gap discontinuity with 0.43 mm coupling length

The edge-coupled NRD guide discontinuity is shown in figures 2.8 and 2.9 of chapter 2. The FDTD parameters are listed in table 4.5. The simulation has been performed in the same manner as for the previous cases.

The magnitudes of the scattering parameters S_{11} and S_{12} calculated through the processing of the time-domain results are shown in figure 4.17 and the corresponding phases are given in 4.18.

Table 4.4 FDTD parameters for end-coupled gap discontinuity with 1.72 mm gap

S. No.	FDTD Parameter	Symbol	Numerical Value
1	Velocity of EM wave in free space	c	299792458 m/s
2	Permeability	μ_0	$4\pi \times 10^{-7}$ henry/m
3	Permittivity of free space	ε_0	8.854×10^{-12} F/m
4	Relative Dielectric constant (Alumina)	ε_r	9.5
5	Frequency	f_c	35 GHz.
6	Space step in Yee's cell	Δ	0.43 mm
7	Time step	Δt	0.2678 ps
8	Width	a	3.86 mm
9	Thickness	b	1.32 mm
10	Length	l	10.29 mm
11	Length of each dielectric strip	m	4.29 mm
12	Width of the front face	w	3.00 mm
13	Gap width	p	1.72 mm
14	No. of cells along width (Z-dir.)	n_z	9
15	No. of cells along thickness (Y-dir.)	n_y	7
16	No. of cells along length (X-dir.)	n_x	24
17	Source excitation (Gaussian in space and time) [Electric]	S_0	$E_0 e^{\left(-\left(\frac{t-20\Delta t}{10\Delta t}\right)^2\right)}$ $(E_0 = 1)$

Fig. 4.15 Magnitude of S_{11} and S_{12} of end-coupled NRD guide with 1.72 mm gap.

4.16 Phase of S_{11} and S_{12} versus frequency of 1.72 mm gap coupled NRD guide.

Table 4.5 FDTD parameters for edge-coupled gap discontinuity with 0.43 mm coupling length.

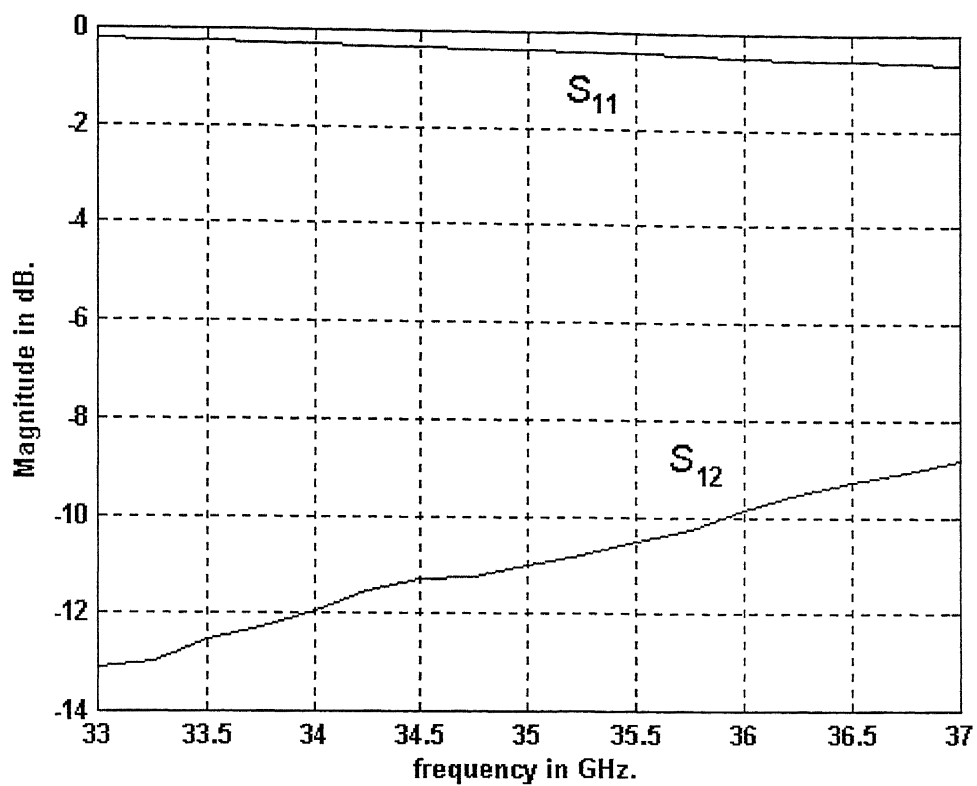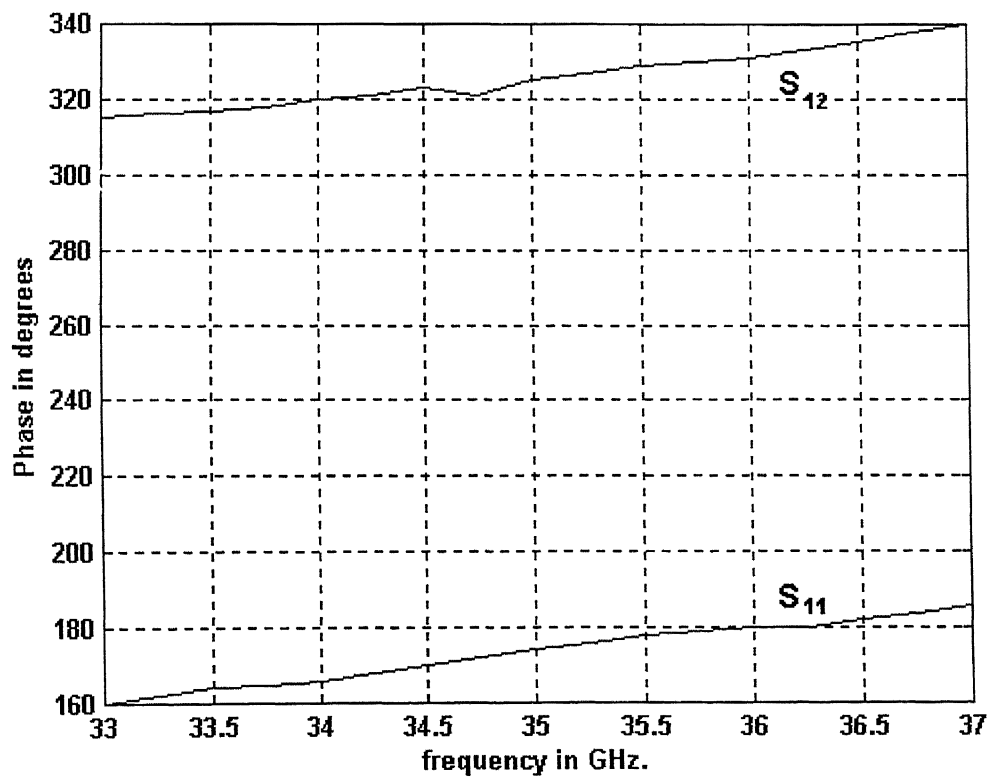| S. No.	FDTD Parameter	Symbol	Numerical Value
1	Velocity of EM wave in free space	c	299792458 m/s
2	Permeability	μ_0	$4\pi \times 10^{-7}$ henry/m
3	Permittivity of free space	ε_0	8.854×10^{-12} F/m
4	Relative Dielectric constant (Alumina)	ε_r	9.5
5	Frequency	f_c	35 GHz.
6	Space step in Yee's cell	Δ	0.43 mm
7	Time step	Δt	0.2678 ps
8	Width	a	3.86 mm
9	Thickness	b	1.32 mm
10	Length	l	8.14 mm
11	Length of each dielectric strip	m	4.29 mm
12	Width of the front face	w	4.71mm
13	Gap width	q	0.43 mm
14	Coupling length	p	0.43 mm
15	No. of cells along width (Z-dir.)	n_z	9
16	No. of cells along thickness (Y-dir.)	n_y	11
17	No. of cells along length (X-dir.)	n_x	19
18	Source excitation (Gaussian in space and time) [Electric]	S_0	$E_0 e^{\left(-\left(\frac{t-20\Delta t}{10\Delta t}\right)^2\right)}$ $(E_0 = 1)$
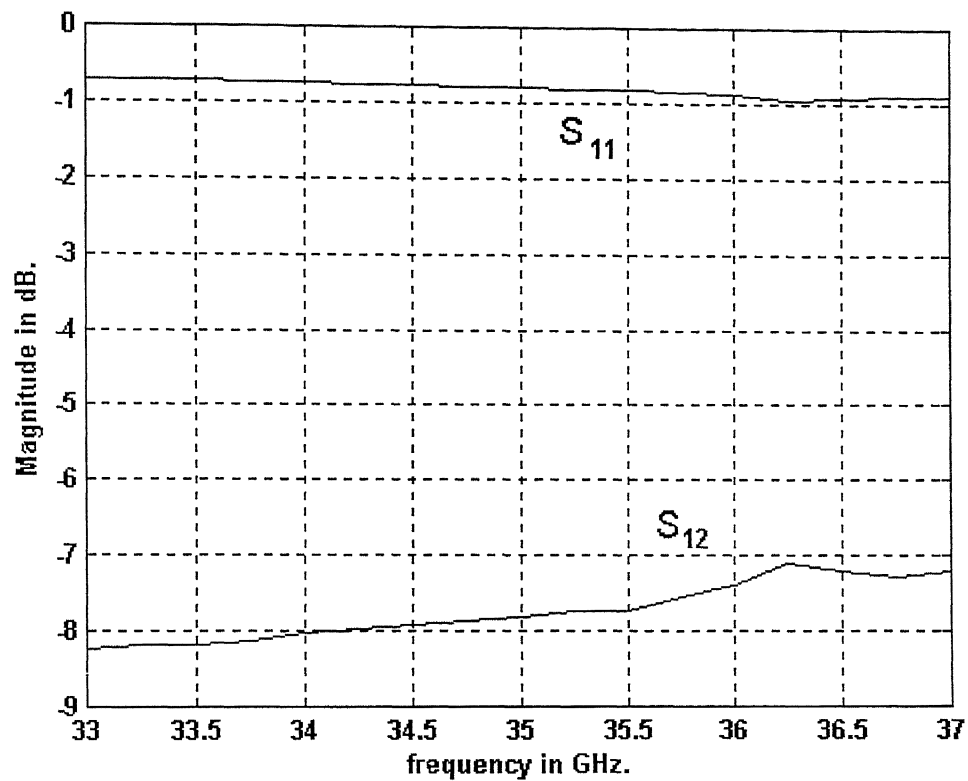
Fig. 4.17 Magnitude of S_{11} and S_{12} of edge-coupled NRD guide with 0.43mm coupling length.
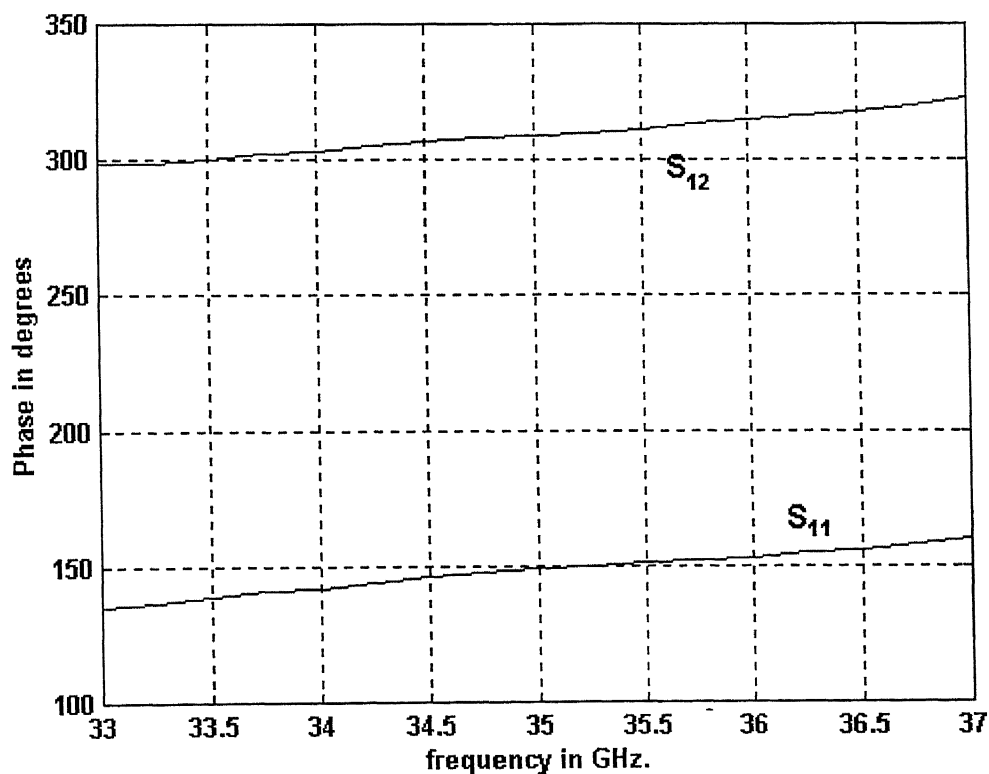

Fig. 4.18 Phase information of 0.43mm edge-coupled NRD guide

4.6.2 Edge-coupled gap discontinuity with 0.86 mm coupling length

Refer to the same figures as in the previous section for the end-coupled NRD guide discontinuity. The corresponding FDTD parameters are listed in table 4.6. The magnitudes of the frequency dependent scattering parameters S_{11} and coefficient S_{12} are shown in figure 4.19 and the corresponding phase is shown in figure 4.20.

Refer to figure 4.19 where the reflection and the transmission coefficients of the NRD guide edge-coupled discontinuity with 0.86 mm coupling length is shown and figure 4.13 where the same parameters are plotted for and end-coupled gap with the same coupling length. By comparing these two plots, we observe that an edge-coupled non radiative dielectric waveguide discontinuity has better coupling characteristics as against an end coupled non radiative dielectric waveguide discontinuity under similar conditions. As done with the mictrostrip lines, cascaded edge-coupled guides can be used to design filters with NRD guides.

Finally, we present a few general points to be remembered while carrying an FDTD simulation:

- The three dimensional FDTD simulations involve the updation of a huge number (sometimes millions [2]) of field components in each iteration. This will impose severe load on the CPU and the RAM. If the simulation is being carried out in MATLAB, 64 MB or higher RAM is suggested. Processor of 500 MHz. or faster is recommended. Memory requirements are also higher as large amount of data is stored in each iteration.

- As stated earlier, stability of the simulation must be taken care of. A lower value of the stability factor is taken when dielectrics are also present inside the computational domain.

Table 4.6. FDTD parameters for edge-coupled gap discontinuity with 0.86 mm coupling length.

| S. No.	FDTD Parameter	Symbol	Numerical Value
1	Velocity of EM wave in free space	c	299792458 m/s
2	Permeability	μ_0	$4\pi \times 10^{-7}$ henry/m
3	Permittivity of free space	ε_0	8.854×10^{-12} F/m
4	Relative Dielectric constant (Alumina)	ε_r	9.5
5	Frequency	f_c	35 GHz.
6	Space step in Yee's cell	Δ	0.43 mm
7	Time step	Δt	0.2678 ps
8	Width	a	3.86 mm
9	Thickness	b	1.32 mm
10	Length	l	7.71 mm
11	Length of each dielectric strip	m	4.29 mm
12	Width of the front face	w	4.71 mm
13	Gap width	q	0.43 mm
14	Coupling length	p	0.86 mm
15	No. of cells along width (Z-dir.)	n_z	9
16	No. of cells along thickness (Y-dir.)	n_y	11
17	No. of cells along length (X-dir.)	n_x	18
18	Source excitation (Gaussian in space and time) [Electric]	S_0	$E_0 e^{\left(-\left(\frac{t-20\Delta t}{10\Delta t}\right)^2\right)}$ $(E_0 = 1)$
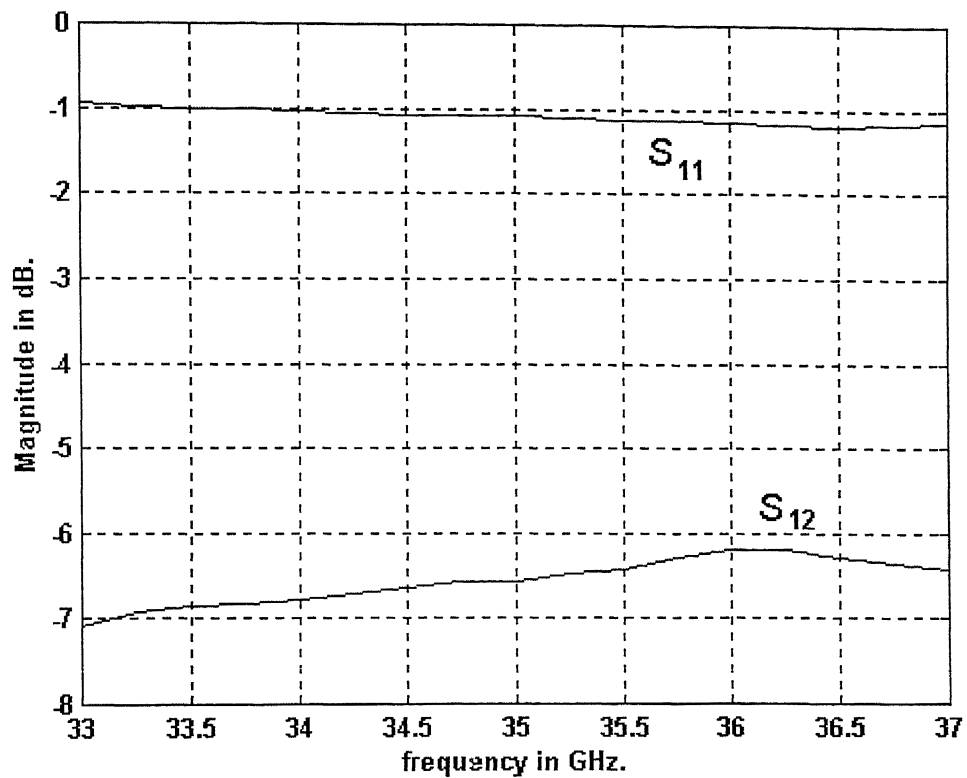
Fig. 4.19 Magnitude of S_{11} and S_{12} of 0.86 mm edge –coupled NRD guide.
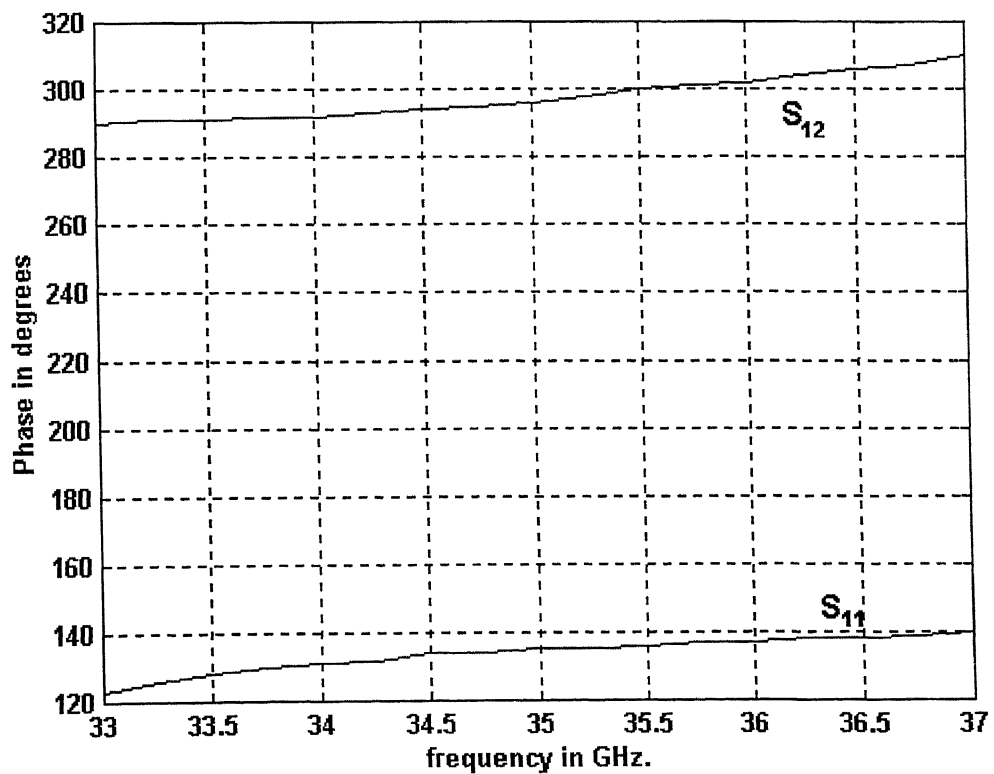

Fig. 4.20 Phase information of the 0.86 mm edge-coupled NRD guide.

Chapter 5

Summary and Conclusions

5.1 Summary

Analysis of the non radiative dielectric waveguide (NRD) discontinuities by the finite-difference time-domain (FDTD) technique was presented in the thesis. The non radiative dielectric waveguide consists of a dielectric strip of rectangular cross-section sandwiched between two parallel conducting plates. Most of the electromagnetic energy is concentrated in the dielectric strip. The presence of a discontinuity in a guide may launch several modes, which are unpredictable. As the rigorous analysis is very difficult, one opts for a computational method.

The principle of operation and the properties of the NRD guide are presented in chapter2. The NRD guides have a lower attenuation than the conventional rectangular waveguides. Since NRD fields decay very fast outside the dielectric strip, bends and discontinuities can be easily incorporated with little radiation. The low losses of NRD guides make them suitable for millimeter wave frequencies. The design procedure and the derivation of *LSE* and *LSM* modes are outlined. The dimensions of the NRD guides over a range of frequencies for

three dielectrics namely Alumina ($\varepsilon_r = 9.5$), Fused quartz ($\varepsilon_r = 3.8$) and Teflon ($\varepsilon_r = 2.1$) are calculated. The description of the open-end, end-coupled gap and the edge-coupled NRD guide discontinuities is also given in the second chapter.

Yee [1] originated a set of finite-difference equations for the time dependent Maxwell's curl equations system. The Yee algorithm solves for both electric and magnetic fields in time and space using the coupled Maxwell's curl equations rather than solving the electric field alone (or magnetic field alone) with a wave equation.

The third chapter is devoted to the FDTD technique. The salient features of FDTD method are discussed. In the FDTD formulation part, the expressions for the central differencing scheme are given. Using these expressions, Maxwell's equations are discretized and all the finite difference equations for electric and magnetic field components in rectangular coordinate system are derived. The FDTD simulation involves the division of the computational domain into a large number of small cuboids called Yee's cells. Each cell has field components associated with it which are modified in each run of the simulation. These modified values in the cells are used to calculate the field components in the next run. Hence any error in calculation will propagate very rapidly giving absurd results. The conditions on the space and time steps to ensure stability of the simulation are discussed in the thesis.

Special treatment is needed for the open boundaries, if any in the structure under analysis. This is because one cannot have infinite computing domain. Special boundary conditions called absorbing boundary conditions (ABCs) are used for the purpose. ABCs truncate the computing domain by absorbing the incident waves and thereby simulating the infinite space at the open boundaries. The thesis discusses the ABCs and presents an analytical ABC proposed by Mur [7]. Generally, one is interested in the frequency-domain characteristics of the electromagnetic structure such as the scattering parameters, resonant frequency etc. The procedure to obtain the frequency domain characteristics from the time-domain data is described.

The fifth chapter has the results and discussion part. After the FDTD simulation code has been written, we tested it for the problem similar to the one given by Yee [1] in his paper: Scattering of an incident TM wave by an obstacle. The simulation has been performed for the open-ended, end-coupled and edge-coupled NRD guide discontinuities. Frequency dependent scattering parameters of each discontinuity modeled as a two-port network are calculated.

5.2 Conclusions

It is shown in the thesis that, the FDTD technique can be applied to NRD guides. The results obtained through the FDTD simulation of the NRD guide discontinuities could not be verified theoretically, as the published results are not available in this case. We tested the code we developed by applying it to the problem of the scattering of an incident TM wave by a square obstacle, which was similar to the one proposed by Yee [1] in his paper. The testing results gave satisfying results, keeping in view the changes we made to the original problem After carrying out the simulation with different stability factors (discussed in chapter 4), it is observed that the simulation results are erroneous if the stability factor S, exceeds one.

5.3 Scope for further work

This thesis investigates the behavior of NRD guide discontinuities through a computational method. The scope for extending the present work lies in:

- The analysis of end-coupled and edge-coupled NRD guides has been done for two gap widths for the former and two coupling lengths for the later case. This is not enough to generate the complete design data. For the design, one needs the impedance curves as a function of gap width or coupled lengths. One has to carry the simulation for considerable number of gap or coupled lengths and use curve-fitting and interpolation techniques to obtain the design curves.
- One can use the discontinuity data generated in the design of various NRD guide devices such as couplers filters and power dividers.

- The NRD guide discontinuities analysed in the thesis were not curved. This makes the FDTD formulation in rectangular coordinate system straightforward. Some devices like directional couplers and power dividers may have curved boundaries and their FDTD formulation is tedious in the cartesian coordinate system. Alternatively, one may go for the formulation in rotationally symmetric coordinate systems.

- To reduce the computational time, one can restrict the fine grid only to the region nearer to the discontinuity. A course grid can be used for other regions inside the volume, thereby reducing the total number of cells inside the volume and hence the computational time.

- An unconditionally stable FDTD algorithm called alternating direction implicit (ADI) FDTD technique has been proposed recently [22], which may solve the problems associated with the stability of the simulation. This can be incorporated into the code.

References

[1] K.S. Yee, "Numerical solution of initial boundary value problems involving Maxwell's equations in isotropic media," *IEEE Trans. Antennas propagat.,* vol. AP-14, no. 4, pp. 302-307, May 1996

[2] Allen Taflove and Susan C. Hagness, *Computational Electrodynamics, The finite difference time-domain method,* Artech House, Norwood, MA, 2000.

[3] K.L. Shlager and J B. Schnieder, "A selective survey of the finite difference time-domain literature," *IEEE Trans. Antennas Propagat.,* vol. APM-37, no.4,pp. 39-56, April 1995.

[4] Allen Taflove and M.E. Brodwin, "Numerical solution of steady state electromagnetic scattering problems using the time-dependent Maxwell's equations," *IEEE Trans. Microwave Theory Tech.,* vol. MTT-23, no. 8, pp. 623-630, August 1975.

[5] Xiaolei Zhang and Kenneth K. Mei, "Time-domain finite difference approach to the calculation of the frequency-dependent characteristics of microstrip discontinuities," *IEEE Trans. Microwave Theory Tech.,* vol. 36 no. 12, pp. 1775-1787, December 1988.

[6] B. Enquist and A. Mazda, "Absorbing boundary conditions for the numerical simulation of waves," Mathematics of computation, vol. 31, pp. 629-651, 1977.

[7] G. Mur, "Absorbing Boundary Conditions for the finite-difference approximation of the time-domain electromagnetic equations," *IEEE Trans. on Electromagnetic Compatibility,* vol. EMC-23, no. 4, pp. 377-382, November 1981.

[8] R. Hallond and J.W. Williams, "Total field versus scattered field finite difference codes: A comparative assessment," *IEEE Trans on Nuclear Science,* vol. NS-30, no. 6, pp. 4583-4588, December 1983.

[9] Xiaolei Zhang, Jiayuan Fang and Kenneth K. Mei, "Calculations of the dispersive characteristics of microstrips by the time-domain finite difference method," *IEEE Trans. Microwave Theory Tech.,* vol.36, no. 2, pp. 263-267, February 1988.

[10] David M. Sheen, Sami M. Ali, Mohamed D. Abouzahra and J.A. Kong, "Application of the finite-difference time-domain method to the analysis of planar microstrip circuits," *IEEE Trans. Microwave Theory Tech.,* vol. 38, no. 7, pp. 849-856, July 1990.

[11] Yinchao Chen, Raj Mittra and Paul Harms, "Finite-difference time domain algorithm for solving Maxwell's equations in rotationally symmetric geometries," *IEEE Trans. Microwave Theory Tech.,* vol. 44, no. 6, pp. 832-839, June 1996.

[12] Svetlana S. Zivanovic, Kane S. Yee and Kenneth K. Mei, "A subgridding method for the time-domain finite-difference method to solve Maxwell's equations," *IEEE Trans. Microwave Theory Tech.*, vol. 39, no. 3, pp. 471-479, March 1991.

[13] Guoqiang Shen, Yinchao Chen, and Raj Mittra, " A non-uniform FDTD technique for efficient analysis of propagation characteristics of optical-fiber waveguides," *IEEE Trans. Microwave Theory Tech*, vol. 47, no. 3, pp. 345-349, March 1999.

[14] Mohammed F. Hadi and Melinda Picket May, "A modified FDTD (2,4) scheme for modeling electrically large structures with high-phase accuracy," *IEEE Trans. Antennas Propagat*, vol. 45, no.2, pp 254-264, February 1997.

[15] Kang Lan, Yaowu Liu, and Weigan Lin, "A higher order (2,4) scheme for reducing dispersion in FDTD algorithm," *IEEE Trans. on Electromagnetic Compatibility*, vol. 41, no. 2, pp. 160-165, May 1999.

[16] Tsukasa yoneyama, Shigeo Nishida, "Nonradiative Dielectric Waveguide for millimeter-wave integrated circuits," *IEEE Trans Microwave Theory Tech.*, vol. MTT-29, no. 11, pp. 1188-1192, November 1981.

[17] Tsukasa Yoneyama, Norio Tozawa and Shigeo Nishida, "Coupling characteristics of nonradiative dielectric waveguides," *IEEE Trans. Microwave Theory Tech.*, vol. MTT-31, no.8, pp. 648-654, August 1983.

[18] R.E. Collin, *Field Theory of Guided Waves*, chapter 6, pp. 224-257, McGraw-Hill Book Company Inc., New York, 1960.

[19] Debasis Dawn, "Analysis and design of Nonradiative Dielectric Waveguide and its excitation," M.Tech thesis, Indian Institute of Technology, Kanpur, Department of Electrical Engineering, Kanpur, India, August 1989.

[20] Andrew F. Peterson, Scott L. Ray and Raj Mittra, *Computational Methods for Electromagnetics*, IEEE Press, New York, 1988.

[21] K.C. Gupta, Ramesh Garg, and Rakesh Chadha, *Computer-aided design of Microwave circuits*, Artech House, Norwood, MA, 1981.

[22] Zheng, F., Z. Chen, and J. Zhang, "Towards the development of a three-dimensional unconditionally stable finite-difference time-domain method," *IEEE Trans. Microwave Theory Tech.*, vol. 48, 2000 (in press).